Stability analysis of thin-walled steel structures

Interaction between local and global buckling modes

Miguel Castro Fonseca Pinto da Costa

Thesis to obtain the Master of Science Degree in

Integrated Master Degree (MSc) in Civil Engineering

Supervisors

Prof. Dr. Ricardo José de Figueiredo Mendes Vieira

Prof. Dr. Francisco Baptista Esteves Virtuoso

Examination Committee

Chairperson: Prof. Dr Fernando Manuel Fernandes Simões

Supervisor: Prof. Dr. Ricardo José de Figueiredo Mendes Vieira

Member of the Committee: Prof. Dr Manuel da Cunha Ritto Corrêa

October 2014

Abstract

The present work has the purpose to contribute to the knowledge of the interaction between local and global (flexural) buckling modes and its effects on the ultimate load of I-columns and its comparison to the Eurocode 3 (EC3) design buckling resistance.

To achieve such knowledge, local and global buckling modes were studied. Beginning with local buckling and thin plate's theory, the study started with two examples: a simply supported plate and a plate with one longitudinal free edge. Then, the I-column was studied and its local buckling load was derived. The global buckling was studied concerning beam's theory and the Euler's buckling load.

A geometrical non-linear analysis was performed by using Abaqus software. The analysis was performed based on a particular I-column with uncommon dimensions in order to study the interaction between buckling modes. Notice that no torsional buckling mode was allowed.

It was verified that the interaction between local and global buckling modes occurred, having more impact for lower slenderness ratios of the column, though the column's behavior became unstable for the range of lengths analyzed. Another conclusion was that interaction between global buckling modes also occurred, however, its impact was more significant for higher values of the column's slenderness.

Regarding the design buckling loads from the EC3, it predicts with a safe margin the ultimate load for lower values of the column's slenderness. However, for higher values of the slenderness ratio of the column, the EC3 may fail to take into consideration the interaction between global modes.

Keywords: Plates; Columns; Stability; non-linear analysis; Geometric imperfections; Eurocode 3.

Resumo

A presente dissertação tem como objectivo aprofundar o conhecimento sobre a interacção entre modos de encurvadura locais e globais (de flexão) e as suas consequências relativamente à carga última e a sua comparação com a carga resistente definida pelo Eurocódigo 3.

Para atingir o objectivo proposto, utilizou-se a teoria de placas finas e estabilidade das mesmas, centrando-se em dois exemplos: uma placa simplesmente apoiada e uma placa com um bordo longitudinal livre. Depois, a secção em I foi estudada e a sua carga crítica foi calculada. A encurvadura global foi estudada tendo em conta a teoria de peças lineares e a sua correspondente carga de Euler.

Foi feita uma análise geometricamente não-linear de uma coluna através do software Abaqus.

A análise centrou-se no estudo de uma coluna em I com uma secção transversal particular, de modo a ter cargas críticas para os modos globais e local bastante semelhantes. Não se considerou o efeito da torção.

Concluiu-se que existe interacção entre os modos local e globais, especialmente para valores reduzidos da esbelteza da coluna em análise, sendo que a interacção provocou instabilidade. Verificou-se também interacção entre modos de encurvadura globais.

Relativamente à resistência de encurvadura definida pelo EC3, o seu objectivo é cumprido, de forma conservativa, para colunas pouco esbeltas. Porém, o EC3 pode ser passível de falhas no cálculo da resistência para colunas com esbeltezas elevadas, pois não contabiliza a interacção entre modos globais devido à introdução de imperfeições geométricas globais nos dois eixos de flexão da coluna.

Palavras-chave: Placas; Colunas; Estabilidade; Análise não-linear; Imperfeições geométricas; Eurocódigo 3.

Acknowledgment

My deeply acknowledgment and recognition to my supervisors: Professor Ricardo Vieira and Professor Francisco Virtuoso, for all the dedication, patience and time spent during this thesis. I am also profoundly grateful for the possibility given by them to increase my knowledge on this particular fascinating subject.

I would like to thank my parents and sister for the support during this thesis and the five years of university experience and never doubting of my capacities. I am also very thankful for being able to study what I wanted. My thanks go also to the rest of my family, particularly to my grandmother and my aunt Ana.

Finally, many thanks to all my friends, especially the ones that I had the opportunity to come across during these academic years.

Contents

List of Figures

List of Tables

List of Symbols and Acronyms

Symbols and acronyms are usually defined with its first appearance. Tough, to make clear all doubts regarding it, their definition will be presented.

Symbols

w	Plate's deflection
κ_{xx}	Bending strain in x-axis
κ_{yy}	Bending strain in y-axis
ρ_{xy}	Shear strain
m_{xx}	Bending moment in x-axis
m_{yy}	Bending moment in y-axis
m_{xy}	Twisting moment
D	Flexural stiffness
ν	Poisson's ratio
E	Young's modulus
t	Plate's thickness
q	Distributed lateral load
N_x	Edge compressive force in x-direction
N_y	Edge compressive force in y-direction
N_{xy}	Edge shearing force
a	Plate's length
b	Plate's width / flange's width
σ_x	Stress in the x-direction
m	Number of sinusoidal half-waves
σ_{cr}	Buckling stress
ϕ	Aspect ratio
K	Stress parameter
∇^4	Biharmonic operator
F	Stress function
ε	Membrane strains / initial imperfection's parameter
C	Axial stiffness
w^0	Initial deflection
$\bar{q}$	Deflection's amplitude normalized by the plate's thickness
P_{cr}	Buckling load
I	Moment of inertia
L	Column's length
$P_{cr,eff}$	Effective buckling load
G	Shear modulus
A	Cross-sectional area
A_{eff}	Effective cross-sectional area
δ	Maximum transversal displacement of the column
P	Applied axial load
σ_y	Yielding stress
h	Web's width
t_w	Web's thickness
t_f	Flange's thickness
$\overline{\lambda_z}$	Non-dimensional slenderness about axis z
$\overline{\lambda_y}$	Non-dimensional slenderness about axis y

$P_{cr,local}$	Local buckling load
$P_{cr,global,z}$	Global (flexural) buckling load about axis z
$P_{cr,global,y}$	Global (flexural) buckling load about axis y
$N_{b,Rd}$	Design buckling resistance by the EC3
P_u	Ultimate load capacity
v	Displacement along the y-direction
w	Displacement along the z-direction
W_z	Section modulus about z-axis
W_y	Section modulus about y-axis
v_0	Initial displacement along y-direction
w_0	Initial displacement along z-direction
σ_N	Normal stress due to the axial load
σ_{My}	Normal stress due to bending about y-axis
σ_{Mz}	Normal stress due to bending about z-axis
σ_{total}	Total normal stress
i_y	Radius of gyration about y-axis
I_{yy}	Moment of inertia about y-axis
λ_y	Slenderness about y-axis
i_z	Radius of gyration about z-axis
I_{zz}	Moment of inertia about z-axis
λ_z	Slenderness about z-axis
χ	Reduction factor for relevant buckling mode
α	Imperfection factor
ϕ	Value to determine the reduction factor
γ_{M1}	Partial factor for resistance of members to instability assessed by member checks
$L_{cr,z}$	Buckling length about z-axis
$L_{cr,y}$	Buckling length about y-axis
$\overline{\lambda_p}$	Plate slenderness
k_σ	Buckling factor
ψ	Stress ratio
ρ	Reduction factor for plate buckling
b_{eff}	Effective width

Acronyms

EC3	Eurocode 3
FE	Finite element

1 Introduction

Thin-walled steel structures are widely used around the world. From ships, aircrafts to bridges and industrial buildings. These types of steel structures, due to the cost of the material and the developments of more resistant materials, are becoming more and more slender.

The increase of the ratio between the width of the elements and its thickness in thin-walled steel structures is increasing the interest of the investigators regarding local buckling phenomenon (Macdonald, Heiyantuduwa, & Rhodes, 2008).

Thin-walled steel structures are usually open section, being very flexible to torsion due to its low torsional stiffness. So torsional buckling could be important to these types of structures, without forgetting the important of global (flexural) buckling.

All these types of buckling modes are well investigated specially for cold-formed steel lipped-sections (Schafer, March 2002). A lot less investigation was performed for I-columns.

However, even with these types of buckling modes well studied, interaction between buckling modes can arise. It depends on the cross-section geometry, the column's length, and boundary conditions among other factors.

The interaction between buckling modes can have a significant change on the structure's behavior. Local buckling has a stable path and a significant increase of the post-buckling strength of its plate members. Global buckling and its post-buckling behavior are also stable (Bulson & Allen, 1980). But when interacting together the structure's behavior can be so different that interaction between buckling modes is important to consider when designing thin-walled steel structures.

Some investigations was performed regarding interaction between buckling modes for thin-walled lipped channel columns (Anbarasu & Sukumar, 2014) and for thin-walled steel box columns (Kiymaz, 2005) but few were done for I-columns.

In addition to the fact that few studies were focused on I-columns, this thesis was also done with great interest on the design guidelines for this type of steel structures.

The wide use of thin-walled open section steel structures demands an appropriate and simple safety code in order to obtain the design buckling loads. For that reason several codes are being used around the world: North American and European design codes among others.

The Eurocode 3 (EN 1993-1-1:2005) has a simple method to obtain the design buckling resistance of a compressed member based on the geometric and material properties. Being a simplified method, it is extremely important that the results given by the Eurocode 3 are conservative and the method should be able to take into consideration all the buckling phenomenons and their interactions that could reduce the ultimate load of the structure.

So, local and global flexural buckling modes will be studied. Then the interaction between modes will be analyzed with the help of a finite element model. Afterwards, a comparison between the ultimate loads from the finite element model and the Eurocode design loads will be performed in order to verify the Eurocode 3 design guidelines and if the European code takes into consideration interaction between buckling modes.

Now that the problem was defined and set in a frame, this thesis has several goals:

- The study of plate's and beam's theory regarding stability and post-buckling;
- The study of interaction between buckling modes with the help of a finite element model;
- The analysis of the Eurocode 3 and its proposals to calculate the design buckling resistances of structures and the comparison between the results obtained when interaction of local and global (flexural) buckling modes occurs with the finite element analysis method (FE model).

So the main purpose is to analyze thin-walled steel structures when interaction between local and global (flexural) buckling modes occurs.

Therefore, this work will be divided into two main frames. The first one (section 2) has all the theory necessary to understand the problem of buckling of thin-walled structures. Notice that the goal is not to derive all the theory but it's just to have an overall view of the theory behind the problem in analysis.

Section 2.1 has important information about buckling of columns regarding the calculations of buckling loads of columns and its post-buckling theory.

Section 2.2 has a general overview of thin plate's theory with an insight of stability of plates and post-buckling theory.

The other main part of this thesis will be regarding the development and modeling of the structures with finite element method (section 3) in order to study the interaction between buckling modes for a thin-walled open section steel I-column. The validation of the finite element model will be performed in section 4.1.1 and 4.1.2

An example of an I-column was defined in section 4, in order to study the interaction between local and global (flexural) buckling modes. The uncommon properties of the column were defined just to have similar local and global (flexural) buckling loads. The comparison between the ultimate load capacity from the finite element model and the design buckling loads defined by the European code will also be achieved in section 4.

Finally the conclusions regarding the interaction between local and global (flexural) buckling modes and the ability of the Eurocode 3 to take into account the interaction between buckling modes will be addressed in section 5.

2 Buckling of thin-walled structures

As it is known, plates and columns have different behaviors after buckling. Plates can have a significant post-buckling strength and its load path is stable. On the other hand, columns have an almost constant stable path with minimal increasing of the load strength after buckling (Bulson & Allen, 1980).

With these two different behaviors between plates and columns, thin-walled structures can be studied in two separate ways. Columns can be analyzed either globally by using beam's theory or be studied by plate's theory by considering the plate elements (web and flanges).

Those two theories are very different. That's why it's so important to have a brief summary of the two theories separately: beam's theory and plate's theory.

As it was said in the introduction (section 0), this section is not an extensive review of the literature about buckling of thin-walled steel open section columns. It's just a brief summary of it. The summary will start on the global buckling of columns and the column's behavior in the post-buckling field. Notice that from now on, global buckling will always be referenced to global flexural buckling and no other global buckling modes will be related to the expression used.

2.1 Global buckling of columns

The global buckling mode of thin-walled structures is analyzed based on the beam model (Euler-Bernoulli beam theory). The Euler-Bernoulli beam theory is used due to the fact that the thin-walled structures presented in this thesis will be considered as linear prismatic bars without in-plane deformations for the global buckling analysis.

Only simply supported columns will be addressed but other supports only change the boundary conditions of the problem and therefore the buckling length.

Notice that a column is a structure with the forces applied in the axial axis and in this case the forces are only compressive forces.

2.1.1 Buckling of columns

The formula used for calculating the critical load for simply supported columns was the Euler's formula derived in 1757:

$$P_{cr} = EI\left(\frac{n\pi}{L}\right)^2 \tag{2.1}$$

Being P_{cr} the buckling load, EI the column's stiffness for a given bending axis, L the buckling length and n the number of half-waves. As the objective is calculating the lowest bifurcation load, the column has only one half-wave so $n = 1$.

Formula (2.1) was derived based on an ideal column so initially the column is perfectly straight and it's compressed by a centrally applied load. The column is also perfectly elastic. Equation (2.1) also doesn't take into account the shear deformation of the column (Timoshenko & Gere, Theory of Elastic Stability, 1961). Due to the geometry of the columns used in the analyses performed to study buckling of thin-walled steel structures, it was verified that the shear deformation had only a small impact on the buckling load. Therefore, shear deformation was not taken into consideration on the evaluation of the global buckling load.

When the load is applied, the column remains straight until it reaches the critical load. When the load reaches the critical load, the column stops being straight and suffers a lateral displacement. Therefore the critical load (equation (2.1)) can be evaluated based on the equilibrium equation in the deformed position (Timoshenko & Gere, Theory of Elastic Stability, 1961), which takes into account the lateral deflection of the column w, the applied load P and the column's stiffness EI.

Notice that from the formula (2.1), both buckling loads corresponding to the two bending axis of the column can be obtained depending only on the column's stiffness and the buckling length.

2.1.2 Post-buckling of columns

The theory behind the derivation of an equation for post-buckling of columns is very complex and as this thesis has not the objective of having all the theory related to buckling written, it was decided to have the simplest information discussed and guiding the most interested ones to the references. A more developed explanation of the theory behind it is present in (Reis & Camotim, 2001).

Koiter (Koiter, 1945) developed the post-buckling theory that gives the equation regarding post-buckling of columns. It involves energetic methods and it leads to the minimization of the total potential energy.

The minimization of the total potential energy allows to calculate the field of displacements. It will be formed by two parts. One is the displacement of the column when the load is equal to the buckling load. It can be easily calculated by the differential equation of equilibrium of a column and its boundary conditions. The other is the residual displacement field.

To obtain the residual displacement field it's necessary to apply the Koiter's theory and at the end, the post-buckling equation for a perfect column is presented by equation (2.2).

$$\frac{P}{P_{cr}} = 1 + \frac{\pi^2}{8}\left(\frac{\delta}{L}\right)^2 \tag{2.2}$$

being δ the maximum transverse displacement of the column. For a simply supported column with an initial geometric imperfection, the equation is given by equation (2.3)

$$\frac{P}{P_{cr}} = \frac{\left(\frac{\delta}{L}\right) + \left(\frac{\pi^2}{8}\right)\left(\frac{\delta}{L}\right)^3}{\left(\frac{\delta}{L}\right) + \left(\frac{\varepsilon}{L}\right)} \tag{2.3}$$

being ε a parameter related to the initial imperfections.

An example of a simply supported column is shown in Figure 2.1. Its properties are defined at Table 2.1 and the buckling occurs by flexure around the minor axis.

Table 2.1: Material and geometric properties of the column.

E (MPa)	210000
v	0.3
L (m)	20
h (m)	1.1
b (m)	1
t_w (m)	0.02
t_f (m)	0.027
I_{zz} (m4)	0.0045
$P_{cr,z}$ (MN)	23.32

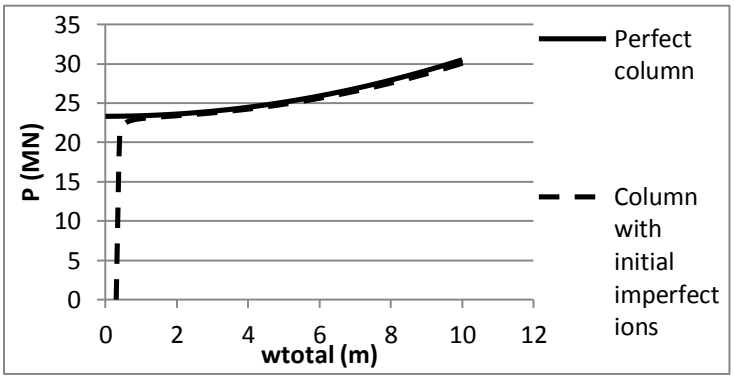

Figure 2.1: Post-buckling path of a perfect column and a column with initial geometric imperfections.

As it's possible to observe from Figure 2.1, the so called Euler column has a stable path after bifurcation.

2.2 Local buckling of columns

The local buckling mode of thin-walled structures is analyzed by the thin plate's theory. After a brief summary of the thin plate's theory, two simple examples of single plates will be addressed: a simply supported plate and a simply supported plate with one longitudinal free edge, since these two plates can represent respectively the web and flange of an I-section. At the end of this present section, the I-section will be analyzed by considering the section as an assemblage of plates (web and flanges).

2.2.1 Thin plates' theory

Before entering into the field of geometrical non-linearity, it's essential to study the bending of thin plates. The theory behind it is the thin plates' theory. It was developed by Kirchhoff in 1850.

This theory is in the field of small displacements. The plate is reduced to its middle plane and all the terms higher than the first order are neglected.

Along with the reduction of the plate to its middle plane, several other assumptions were made by Navier, in 1820 (Timoshenko & Woinowsky-Krieger, Theory of Plates and Shells, 1959):

(i) Deflections are small (less than the thickness of the plate);
(ii) The middle plane of the plate doesn't stretch during bending and remains a neutral surface;

(iii) Plane sections rotate during bending to remain normal to the neutral surface and do not distort, this means the stresses and strains are proportional to their distance from the neutral surface;
(iv) The effect of shear is neglected;
(v) The thickness of the plate is small compared with the others directions.

Then when the plate is in bending, it'll have an effect on both directions of the plate. This effect is due to bending and it is represented by the transverse and longitudinal curvature as well as the twisting of the plate's elements (Bulson & Allen, 1980) and it can be expressed by equation (2.4)

The kinematic condition (2.4), constitutive relation (2.5) and equilibrium equation (2.6) of thin plates are well known, where D is the flexural stiffness of the plate defined in equation (2.7), w is the deflection of the plate, ν is the Poisson's ratio and q is the distributed lateral load on the plate.

$$\begin{cases} \kappa_{xx} = -\dfrac{\partial^2 w}{\partial x^2} \\ \kappa_{yy} = -\dfrac{\partial^2 w}{\partial y^2} \\ \rho_{xy} = -2\dfrac{\partial^2 w}{\partial x \partial y} \end{cases} \tag{2.4}$$

$$\begin{cases} m_{xx} = D(\kappa_{xx} + \nu\kappa_{yy}) \\ m_{yy} = D(\nu\kappa_{xx} + \kappa_{yy}) \\ m_{xy} = \dfrac{D}{2}(1-\nu)\rho_{xy} \end{cases} \tag{2.5}$$

$$-\left(\frac{\partial^2 m_{xx}}{\partial x^2} + 2\frac{\partial^2 m_{xy}}{\partial x \partial y} + \frac{\partial^2 m_{yy}}{\partial y^2}\right) = q \tag{2.6}$$

$$D = \frac{Et^3}{12(1-\nu^2)} \tag{2.7}$$

With these three relations ((2.4)-(2.6)) it's possible to write one single equation (2.8) relating only the deflection of the plate and the distributed load applied on the plate. By substituting equation (2.4) in equation (2.5) it gives the relation between the moments and the displacement. Finally introducing those moments in equation (2.6) it turns out as being the following equation:

$$\left(\frac{\partial^4 w}{\partial x^4} + 2\frac{\partial^4 w}{\partial x^2 \partial y^2} + \frac{\partial^4 w}{\partial y^4}\right) = \frac{q}{D} \tag{2.8}$$

But equation ((2.8**)** only takes into account distributed applied forces on the plate and it can't evaluate the effect of the applied forces at the edges of the plate (Figure 2.2) during its deflection. So, in order to study the effect of forces applied at the edges it is necessary to add those forces to the equation (2.8).

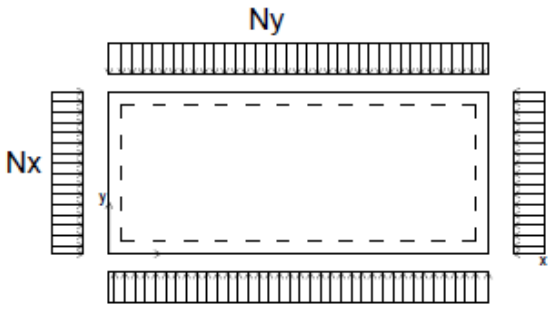

Figure 2.2: Plate with the applied forces at the edges.

By considering that the plate is already subjected to relevant bending, the edge forces applied in the middle plane of the plate will have a vertical and horizontal component.

As assumed at the beginning of this section, it was considered that the displacements of the plate are small so: $\sin(\frac{\partial w}{\partial x}) = \frac{\partial w}{\partial x}$ and the projections of N_x, N_y and N_{xy} are:

$$N_x \frac{\partial^2 w}{\partial x^2} \partial x \partial y$$

$$N_y \frac{\partial^2 w}{\partial y^2} \partial x \partial y$$

$$N_{xy} \frac{\partial^2 w}{\partial x \partial y} \partial x \partial y$$

Now having these projections of the applied forces it is possible to introduce them in the biharmonic equation (2.8) leading to the equation derived by Saint-Venant (2.9) at the end of the XIX century (Bulson & Allen, 1980).

$$\frac{\partial^4 w}{\partial x^4} + 2\frac{\partial^4 w}{\partial x^2 \partial y^2} + \frac{\partial^4 w}{\partial y^4} = \frac{1}{D} * \left(q + N_x \frac{\partial^2 w}{\partial x^2} + 2N_{xy} \frac{\partial^2 w}{\partial x \partial y} + N_y \frac{\partial^2 w}{\partial y^2} \right) \quad (2.9)$$

Now with the differential equation of equilibrium (2.9) it's possible to start analyzing the problem of stability of plates.

2.2.2 Stability of plates

The problem of the stability of plates was addressed in section 2.2.1. This means that a linear analysis both geometrical and physical was performed, in other words, the equilibrium was made in the undeformed position of the plate and the plate was considered as being in the elastic range.

In this section, the physical linear behavior is admitted, but a geometrical nonlinear analysis will be adopted to address the problems of plate buckling. To this end, the equilibrium is now derived considering the plate's deformation.

Mathematically it is possible to determine when buckling takes place because a bifurcation occurs in the solution of the differential equation of equilibrium, being the critical load the load which triggers buckling.

In order to calculate the lowest critical load of plate buckling two methods can be used:

(i) Integrating the differential equation of equilibrium defined in equation (2.9);
(ii) Energy method.

Notice that all the formulation that will be considered assumes that the plate is perfectly flat before loading and remains elastic after bifurcation (Bulson & Allen, 1980).

By considering a solution of equation (2.9) (i) and enforcing boundary conditions, an eigenvalue problem is obtained. Then the solution of the eigenvalue problem allows to evaluate the critical buckling load.

The second method (ii) is a method that uses an approximation for the deflection of the plate.

There are different kinds of methods inside the energy method. In this case, the Rayleigh-Ritz method and the Galerkin method are the most used method. A short review of these two methods is written in the annex A.

2.2.2.1 Simply supported plate

A simple example is considered in order to understand how the critical load of a plate is calculated. For that reason, a simply supported plate on all edges and compressed in one direction (Figure 2.3) will be presented in this section.

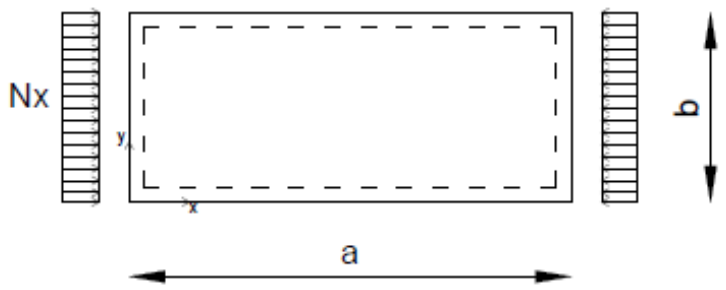

Figure 2.3: Simply supported plate on all four edges with compressive forces in only one direction.

The critical load, in this example, will be obtained from the integration of the differential equation of equilibrium (2.10). Equation (2.11) was introduced on the right-hand side of the equation (2.10) because the plate is under uniaxial compression (x-direction). So equation (2.10) was derived from equation (2.9) and the applied forces are defined in equation (2.11).

$$\frac{\partial^4 w}{\partial x^4} + 2\frac{\partial^4 w}{\partial x^2 \partial y^2} + \frac{\partial^4 w}{\partial y^4} = \frac{1}{D} * \left(\sigma_x t \frac{\partial^2 w}{\partial x^2}\right) \tag{2.10}$$

$$\begin{matrix} N_x = \sigma_x t \\ N_{xy} = 0 \\ N_y = 0 \end{matrix} \tag{2.11}$$

It was assumed that the solution of equation (2.10) was of the following form:

$$w(x,y) = f(y)\sin\left(\frac{m\pi x}{a}\right) \tag{2.12}$$

This solution considers that the plate will buckle into m sinusoidal half-waves in the direction of the compressive loads (x-direction from Figure 2.3). The following figure (Figure 2.4) shows the result of a simply supported plate, uniformly compressed in only one direction and with 3 half-waves that was modeled by the finite element method.

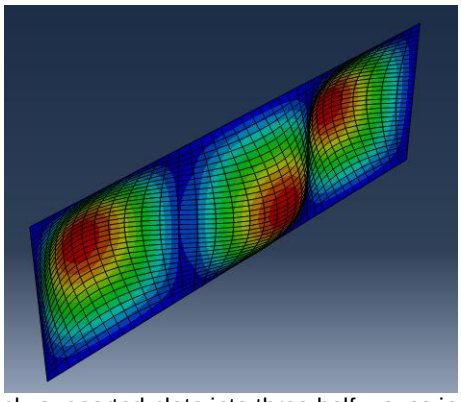

Figure 2.4: Deformation of a simply supported plate into three half-waves in the direction of the compressive force.

By substituting equation (2.12) in equation (2.10), the differential equation is rewritten as follows:

$$\frac{\partial^4 f(y)}{\partial y^4} - 2\left(\frac{m\pi}{a}\right)^2 \frac{\partial^2 f(y)}{\partial y^2} + \left(\left(\frac{m\pi}{a}\right)^4 - \frac{\sigma_x t}{D}\left(\frac{m\pi}{a}\right)^2\right) f(y) = 0 \tag{2.13}$$

The general solution of this differential equation is given by:

$$f(y) = A_1 \cosh(\alpha y) + A_2 \sinh(\alpha y) + A_3 \cos(\beta y) + A_4 \sin(\beta y) \tag{2.14}$$

Being α and β defined by:

$$\begin{cases} \alpha = \sqrt{\left(\frac{m\pi}{a}\right)^2 + \left(\frac{\sigma_x t}{D}\left(\frac{m\pi}{a}\right)^2\right)^{1/2}} \\ \beta = \sqrt{\left(\frac{m\pi}{a}\right)^2 - \left(\frac{\sigma_x t}{D}\left(\frac{m\pi}{a}\right)^2\right)^{1/2}} \end{cases} \tag{2.15}$$

The parameters A_1, A_2, A_3 and A_4 of the solution are obtained by considering the boundary conditions of the plate: two for each border where the loads are applied.

The four boundary conditions to be considered can be written as follows:

$$w(x, 0) = 0 \tag{2.16}$$

$$m_{yy}(x, 0) = 0 \tag{2.17}$$

$$w(x, b) = 0 \tag{2.18}$$

$$m_{yy}(x,b) = 0 \tag{2.19}$$

These boundary conditions correspond to a simply supported plate so there is no deflection along the borders and the borders along $y = 0$ and $y = b$ have no bending moments.

Substituting the solution (2.12) in equations ((2.16)-(2.19)) it turns:

$$(A_1 + A_3)\sin\left(\frac{m\pi x}{a}\right) = 0 \tag{2.20}$$

$$(A_1 p^2 - A_3 q^2)\sin\left(\frac{m\pi x}{a}\right) = 0 \tag{2.21}$$

$$(A_1\cosh(\alpha b) + A_2\sinh(\alpha b) + A_3\cos(\beta b) + A_4\sin(\beta b))\sin\left(\frac{m\pi x}{a}\right) = 0 \tag{2.22}$$

$$(A_1 p^2\cosh(\alpha b) + A_2 p^2\sinh(\alpha b) - A_3 q^2\cos(\beta b) - A_4 q^2\sin(\beta b))\sin\left(\frac{m\pi x}{a}\right) = 0 \tag{2.23}$$

Being the parameters p and q defined by:

$$\begin{cases} p = \sqrt{\alpha^2 - \upsilon\left(\frac{m\pi}{a}\right)^2} \\ q = \sqrt{\beta^2 + \upsilon\left(\frac{m\pi}{a}\right)^2} \end{cases} \tag{2.24}$$

With the purpose of having a non-trivial solution, equations ((2.20)-(2.23)) can be written in a matrix format, allowing to define the bifurcation load by considering the corresponding determinant to be null (equation (2.25)):

$$A\sinh(\alpha b)\sin(\beta b) = 0 \tag{2.25}$$

where the parameter A can be written as follows:

$$A = 2\left(\frac{(m\pi)^2}{\phi}\right)\sqrt{K} \tag{2.26}$$

Being ϕ and K:

(i) the aspect ratio, $\phi = \frac{a}{b}$, i.e. the relation between the plate's length and width;

(ii) K is a parameter that is directly proportional to the critical stress of the plate (equation (2.27) and (2.28)).

$$\sigma = \frac{KD\pi^2}{tb^2} \tag{2.27}$$

That can also be shown as:

$$\sigma_{cr} = \frac{K\pi^2 E}{12(1-\upsilon^2)}\left(\frac{t}{b}\right)^2 \tag{2.28}$$

The parameters αb and βb can be written in a different way in order to show the relation between the coefficients K and ϕ. Notice that the parameter K and ϕ are unidimensional.

$$\begin{cases} \alpha b = \sqrt{\frac{m\pi^2}{\phi}\left(\sqrt{K} + \frac{m}{\phi}\right)} \\ \beta b = \sqrt{\frac{m\pi^2}{\phi}\left(\sqrt{K} - \frac{m}{\phi}\right)} \end{cases} \tag{2.29}$$

So by using the K and ϕ in the equation (2.25) it's possible to evaluate the critical stress (σ_{cr}) of the plate over the increasing of its length.

Finally by fixing the number of half-waves of the deformed shape of the plate and by defining its geometrical properties (a and b) it's possible to calculate K and then the corresponding critical stress.

The critical stress was obtained for several wave lengths and aspect ratios. Figure 2.5 represents how the stresses can change depending on the number of half-waves considered for the plate buckling.

Figure 2.6 has the minimum values of K from each half-wave. It can be observed that the K parameter (or the critical stress σ_{cr}) has an asymptote with value $K \approx 4$ with the increasing of the aspect ratio.

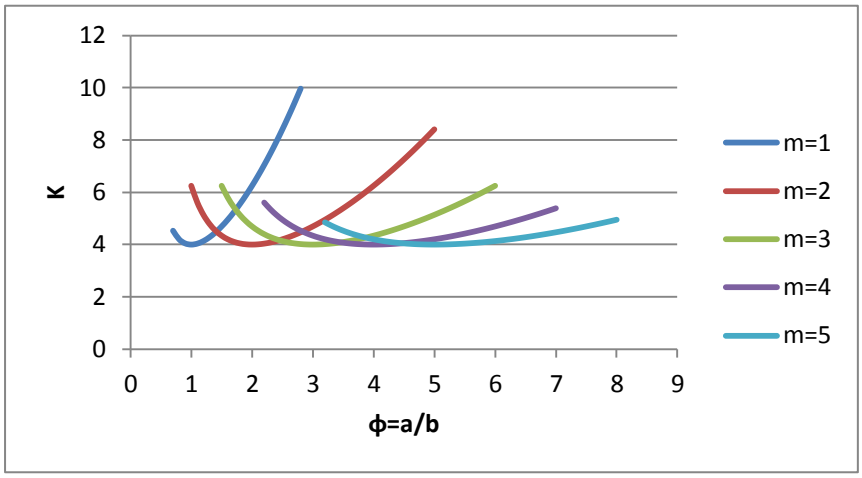

Figure 2.5: Curve K – Φ for simply supported plate.

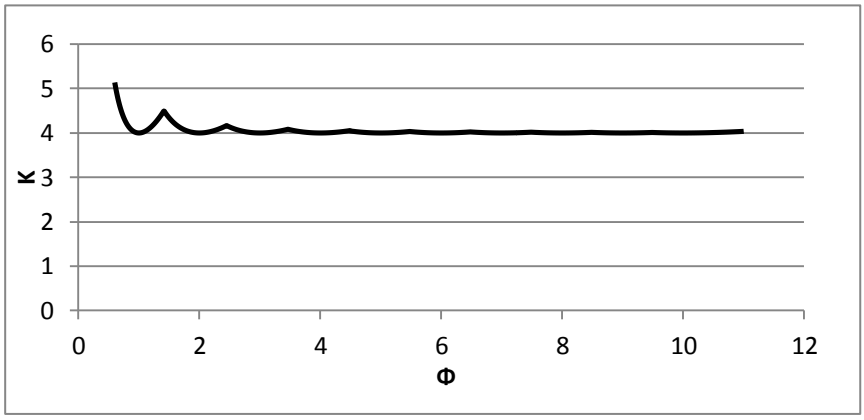

Figure 2.6: Curve K – Φ for simply supported plate with the minimum values of K.

After demonstrating how to obtain the critical stress of a simply supported plate now it's relatively simple to evaluate the local buckling load for every kind of single plate with different boundary conditions, like for example, a plate with longitudinal edges prevented to rotate and its transversal edges simply supported or a plate with one longitudinal edge simply supported and the other free.

In this case, an example where the plate has one longitudinal edge simply supported and the other free with the loading edges simply supported will be analyzed to be possible to compare it between the I section, that will be investigated further, and the simply supported plate.

2.2.2.2 Simply supported plate with one longitudinal free edge

Being the objective the evaluation of the local buckling load for an I-column (section 2.2.2.3) the I-section should be analyzed as an overall plate. To allow a comparison of the I-section, its plates should also be analyzed as single plates (web and flanges).

Analyzing the I-section with its plates in separate, it results in studying a simply supported plate and a plate with one longitudinal edge simply supported and the other free because they can model a web and a flange respectively.

The first case (simply supported plate) was considered in the previous section 2.2.2.1 and the second one (simply supported plate with one longitudinal free edge, Figure 2.7) will be analyzed in this one.

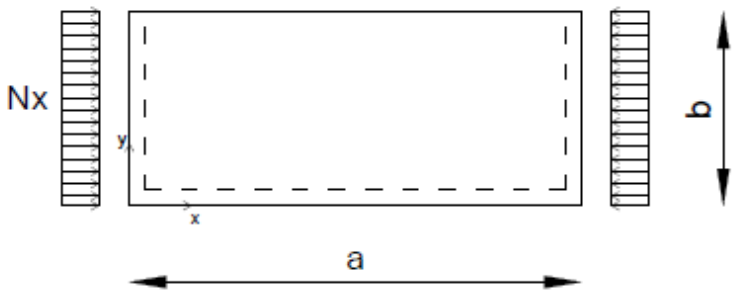

Figure 2.7: plate with one longitudinal edge simply supported and the other free.

The procedure to calculate the critical load is the same as the one adopted for the simply supported plate (section 2.2.2.1). In this case the boundary conditions at the free edge $y = b$ are:

(i) Zero bending moment (2.30);
(ii) Zero shearing force (2.31);

$$m_{yy}(x, b) = 0 \tag{2.30}$$

$$\left(\frac{\partial m_{yy}}{\partial y} + 2\frac{\partial m_{xy}}{\partial x}\right)_{y=b} = 0 \tag{2.31}$$

For the simply supported edge, $y = 0$, the boundary conditions are:

(i) zero deflection (2.32);
(ii) zero bending moment (2.33).

$$w(x,0) = 0 \tag{2.32}$$

$$m_{yy}(x,0) = 0 \tag{2.33}$$

From the section 2.2.2.1, it's known that the general solution of the equilibrium equation (2.34) is:

$$w(x,y) = f(y)\sin\left(\frac{m\pi x}{a}\right) \tag{2.34}$$

Being $f(y)$ defined by:

$$f(y) = A_1\cosh(\alpha y) + A_2\sinh(\alpha y) + A_3\cos(\beta y) + A_4\sin(\beta y) \tag{2.35}$$

So by substituting the solution into the boundary conditions (equations (2.30)-(2.33)), the above equations turn respectively to:

$$(A_1 p^2\cosh(\alpha b) + A_2 p^2\sinh(\alpha b) - A_3 q^2\cos(\beta b) - A_4 q^2\sin(\beta b))\sin\left(\frac{m\pi x}{a}\right) = 0 \tag{2.36}$$

$$\begin{aligned}\Bigg(A_1\,\alpha\sinh(\alpha b)\left(\alpha^2 - (2-\nu)\left(\frac{m\pi}{a}\right)^2\right) + A_2\,\alpha\cosh(\alpha b)\left(\alpha^2 - (2-\nu)\left(\frac{m\pi}{a}\right)^2\right)\\ + A_3\beta\sin(\beta b)\left(\beta^2 + (2-\nu)\left(\frac{m\pi}{a}\right)^2\right)\\ - A_4\beta\cos(\beta b)\left(\beta^2 + (2-\nu)\left(\frac{m\pi}{a}\right)^2\right)\Bigg)\sin\left(\frac{m\pi x}{a}\right) = 0\end{aligned} \tag{2.37}$$

$$(A_1 + A_3)\sin\left(\frac{m\pi x}{a}\right) = 0 \tag{2.38}$$

$$(A_1 p^2 - A_3 q^2)\sin\left(\frac{m\pi x}{a}\right) = 0 \tag{2.39}$$

The parameters p and q are defined in equation (2.24). As well as αb and βb that are defined in equation (2.29).

By writing all the equations ((2.36)-(2.39)) and then setting the determinant of the matrix equal to zero, it's possible to obtain a relation (Figure 2.8) between K and the aspect ratio ϕ.

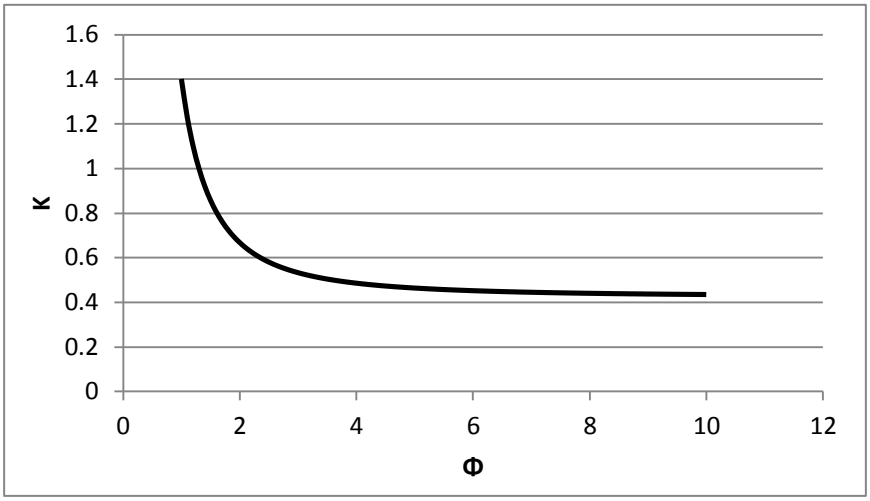

Figure 2.8: Curve K – Φ for a plate with one longitudinal edge simply supported and the other free.

2.2.2.3 I section

The plates that constitute the I-section can be decomposed in two simple examples: a simply supported plate and a simply supported plate with one longitudinal free edge, representing, respectively, the web and the flange. Therefore, the simply supported plate and the simply supported plate with one longitudinal free edge analyzed in section 2.2.2.1 and 2.2.2.2 can be considered as boundaries for the I-section analytical local buckling results when the I-section is considered as an assemblage of plates (web and flanges).

The calculations will be based on the equation of equilibrium as similar as the simply supported plate (section 2.2.2.1) and the plates' deformation is assumed as being like the ones assumed previously (equation (2.12)).

The following figure represents how the plates will deform.

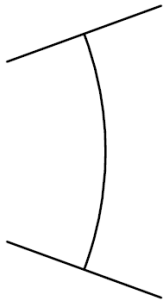

Figure 2.9: Local distortion of an I-section.

An I-section, Figure 2.10, can be analyzed as being an assemblage of plates. By the use of the principles of symmetry, the I-section can be reduced in to two plates: Figure 2.11. The symmetry conditions can be adopted since the local buckling of an I-section has two planes of symmetry.

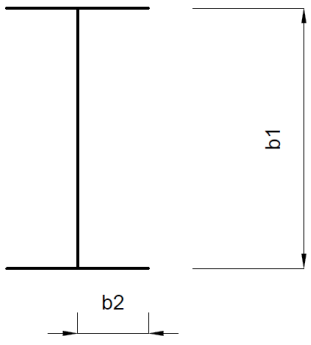

Figure 2.10: I-section

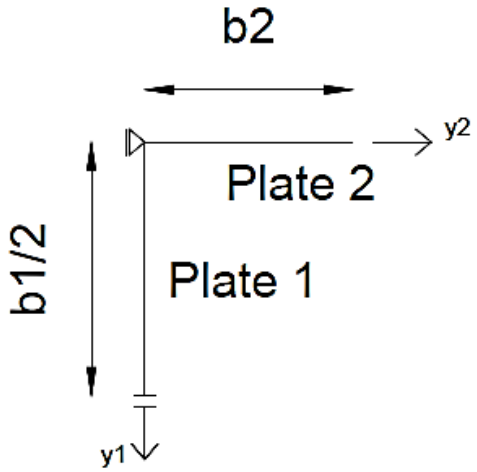

Figure 2.11: I-section after applying the principles of symmetry.

Notice that b_1 and b_2 are the dimensions of the section represented in Figure 2.10, being a the length of the plates.

The loading condition is the same as the ones applied for the two first examples: uniaxial compression (x-direction). The difference lies on the number of boundary conditions to comply, as well as the necessity of ensuring the equilibrium and compatibility between the plates.

For the plate number one alone, the boundary conditions are:

(i) The common edge between plate one and two remains straight during loading so the point $y_1 = 0$ has no deflection, equation (2.40);
(ii) Due to the simplification of symmetry at the middle of the plate one, there won't be any slope, equation (2.41);
(iii) The shear is considered to be null at the middle of the plate, equation (2.42).

$$w_{(y_1=0)} = 0 \tag{2.40}$$

$$\left(\frac{\partial w}{\partial y}\right)_{y_1={}^{b_1}/_2} = 0 \tag{2.41}$$

$$\left(\frac{\partial m_{yy}}{\partial y} + \frac{\partial m_{xy}}{\partial x}\right)_{y_1={}^{b_1}/_2} = 0 \tag{2.42}$$

For the plate number two, the boundary conditions are quite similar:

(i) Like plate one, the common edge remains straight at the point $y_2 = 0$, equation (2.43);
(ii) Since the plate has a free edge, its bending moment at that position is null, equation (2.44);
(iii) The shear force is also null, equation (2.45).

$$w_{(y_2=0)} = 0 \tag{2.43}$$

$$\left(m_{yy}\right)_{y_2=b_2} = 0 \tag{2.44}$$

$$\left(\frac{\partial m_{yy}}{\partial y} + 2\frac{\partial m_{xy}}{\partial x}\right)_{y_2=b_2} = 0 \tag{2.45}$$

To restore compatibility (equation (2.46)) and equilibrium (equation (2.47)), between the two plates, it's necessary to have the following conditions, respectively:

(i) The angle between the two plates has to remain the same;
(ii) Equilibrium of moments at the point $y_1 = y_2 = 0$ has to be ensured:

$$\left(\frac{\partial w}{\partial y}\right)_{y_1=0} - \left(\frac{\partial w}{\partial y}\right)_{y_2=0} = 0 \tag{2.46}$$

$$\left(m_{yy}\right)_{y_1=0} + 2\left(m_{yy}\right)_{y_2=0} = 0 \tag{2.47}$$

Now before developing these eight equations (from equation (2.40) to equation (2.47)), it's important to state the assumptions made about the deflection of these two plates.

Local buckling induces the plates of the I-section to buckle with a certain number of half waves along the longitudinal direction. It was assumed that the buckling modes of the plates have the same wavelength with different functions for the deflection.

So, correspondingly, the deflection functions for the plate one: w_1 (equation (2.48)) and two w_2 (equation (2.49)) are:

$$w_1(x,y) = \left(A_1\cosh(\alpha y) + A_2\sinh(\alpha y) + A_3\cos(\beta y) + A_4\sin(\beta y)\right)\sin\left(\frac{m\pi x}{a}\right)_1 \tag{2.48}$$

$$w_2(x,y) = (A_1\cosh(\alpha y) + A_2\sinh(\alpha y) + A_3\cos(\beta y) + A_4\sin(\beta y))\sin\left(\frac{m\pi x}{a}\right)_2 \tag{2.49}$$

Then by substituting both functions on the boundary conditions, by the order shown above, it follows:

$$(A_1 + A_3)\sin\left(\frac{m\pi x}{a}\right)_1 = 0 \tag{2.50}$$

$$\left(A_1\,\alpha\sinh\left(\alpha\frac{b_1}{2}\right) + A_2\alpha\cosh\left(\alpha\frac{b_1}{2}\right) - A_3\beta\sin\left(\beta\frac{b_1}{2}\right) + A_4\beta\cos\left(\beta\frac{b_1}{2}\right)\right)\sin\left(\frac{m\pi x}{a}\right)_1 = 0 \tag{2.51}$$

$$\left(A_1\,\alpha\sinh\left(\alpha\frac{b_1}{2}\right)\left(\alpha^2 - \left(\frac{m\pi}{a}\right)^2\right) + A_2\alpha\cosh\left(\alpha\frac{b_1}{2}\right)\left(\alpha^2 - \left(\frac{m\pi}{a}\right)^2\right) + A_3\beta\sin\left(\beta\frac{b_1}{2}\right)\left(\beta^2 + \left(\frac{m\pi}{a}\right)^2\right) - A_4\beta\cos\left(\beta\frac{b_1}{2}\right)\left(\beta^2 + \left(\frac{m\pi}{a}\right)^2\right)\right)\sin\left(\frac{m\pi x}{a}\right)_1 = 0 \tag{2.52}$$

$$(A_1 + A_3)\sin\left(\frac{m\pi x}{a}\right)_2 = 0 \tag{2.53}$$

$$\left(A_1\cosh(\alpha b_2)\left(\alpha^2 - \nu\left(\frac{m\pi}{a}\right)^2\right) + A_2\sinh(\alpha b_2)\left(\alpha^2 - \nu\left(\frac{m\pi}{a}\right)^2\right) - A_3\cos(\beta b_2)\left(\beta^2 + \nu\left(\frac{m\pi}{a}\right)^2\right) - A_4\sin(\beta b_2)\left(\beta^2 + \nu\left(\frac{m\pi}{a}\right)^2\right)\right)\sin\left(\frac{m\pi x}{a}\right)_2 = 0 \tag{2.54}$$

$$\left(A_1\,\alpha\sinh(\alpha b_2)\left(\alpha^2 - (2-\nu)\left(\frac{m\pi}{a}\right)^2\right) + A_2\,\alpha\cosh(\alpha b_2)\left(\alpha^2 - (2-\nu)\left(\frac{m\pi}{a}\right)^2\right) + A_3\beta\sin(\beta b_2)\left(\beta^2 + (2-\nu)\left(\frac{m\pi}{a}\right)^2\right) - A_4\beta\cos(\beta b_2)\left(\beta^2 + (2-\nu)\left(\frac{m\pi}{a}\right)^2\right)\right)\sin\left(\frac{m\pi x}{a}\right)_2 = 0 \tag{2.55}$$

$$[(\alpha A_2 + \beta A_4)_1 - (\alpha A_2 + \beta A_4)_2]\sin\left(\frac{m\pi x}{a}\right) = 0 \tag{2.56}$$

$$\left[D_1\left(A_1\left(\alpha^2-\nu\left(\frac{m\pi}{a}\right)^2\right)-A_3\left(\beta^2+\nu\left(\frac{m\pi}{a}\right)^2\right)\right)_1 + 2D_2\left(A_1\left(\alpha^2-\nu\left(\frac{m\pi}{a}\right)^2\right)-A_3\left(\beta^2+\nu\left(\frac{m\pi}{a}\right)^2\right)\right)_2\right]\sin\left(\frac{m\pi x}{a}\right) = 0 \quad (2.57)$$

Being the parameters α and β defined by:

$$\alpha=\sqrt{m\pi^2\left(\frac{\sqrt{K}}{ab}+\frac{m}{a^2}\right)} \quad (2.58)$$

$$\beta=\sqrt{m\pi^2\left(\frac{\sqrt{K}}{ab}-\frac{m}{a^2}\right)} \quad (2.59)$$

where b is either b_1 or b_2 according with the plate being analyzed. Notice that the plate's flexural stiffness D_1 and D_2 is related either to plate number one or plate number two.

So for each plate, the only thing that changes in the parameters above is the width, or in another words, b can be b_1 or b_2. Let us not forget about the flexural stiffness D (equation (2.7)) because the plate's thickness can change: the flange can have a different thickness than the web.

The equations ((2.50)-(2.57)) allows to evaluate the bifurcation stress through the definition of the coefficient K. To this end, the equations are written in a matrix format, being the coefficient K associated with the corresponding null determinant.

By proceeding as the same as what was done in section 2.2.2.1, several $K-\phi$ functions were plotted considering the variation of the relation between the two plates' width: b_2/b_1, with the same thickness for the web and flange.

The first curve, Figure 2.12, was defined for a flange with the double of the web's width, this means that: $b_2/b_1=1$. As already referred, the I-section depending on the relation between the dimension of the web and the flanges has the solution limited by the solutions from a simply supported plate (Figure 2.6) or a simply supported plate with a free edge (Figure 2.8).

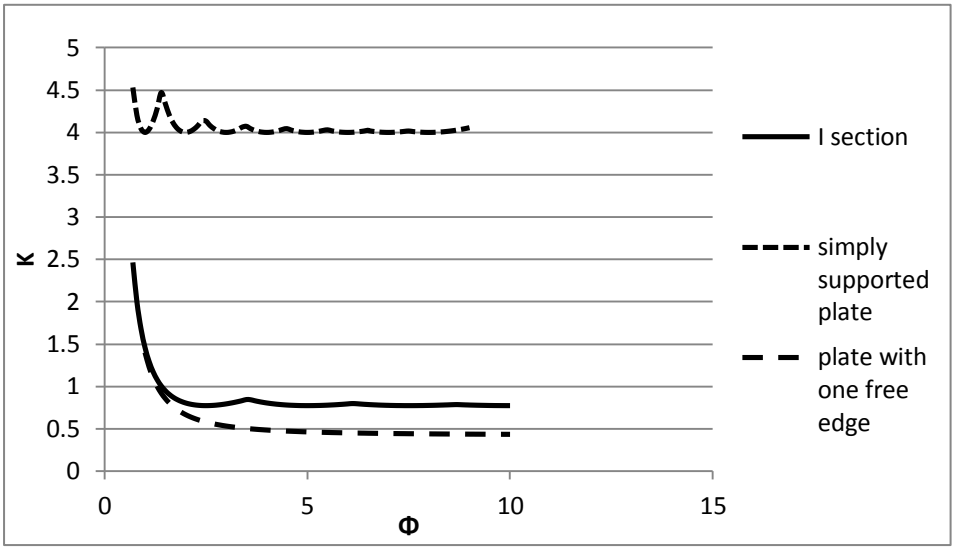

Figure 2.12: Curve K – Φ for I section with b2/b1=1.

For the next curves (Figure 2.13 to Figure 2.17), as the relation b_2/b_1 decreases, the value of K increases. It was expected that for small values of b_2, as the cross-section becomes more like a simply supported plate, the $K - \phi$ curve becomes similar to the Figure 2.6, or K was expected to approach to the value of 4.

However that is not represented in Figure 2.15, Figure 2.16 and Figure 2.17.

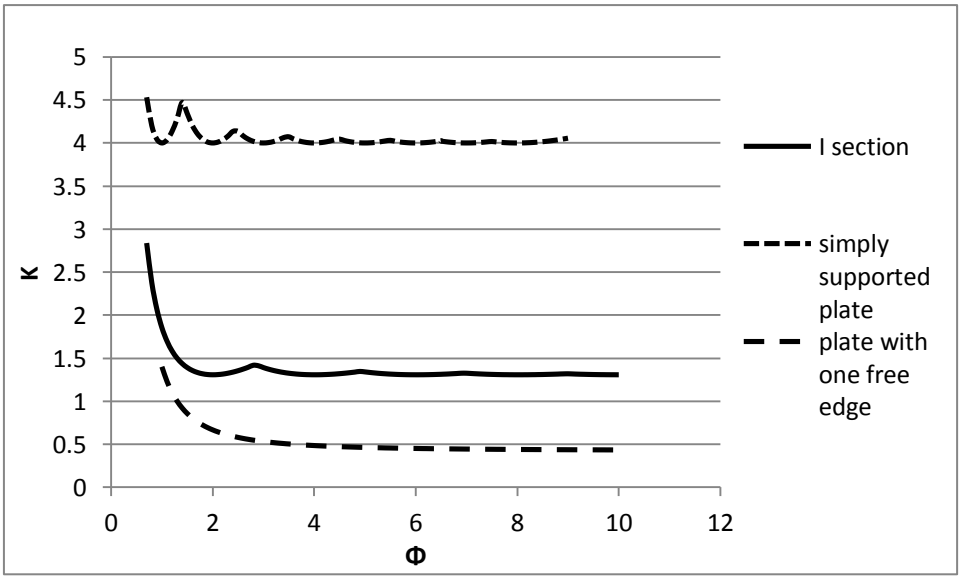

Figure 2.13: Curve K – Φ for I section with b2/b1=0.75.

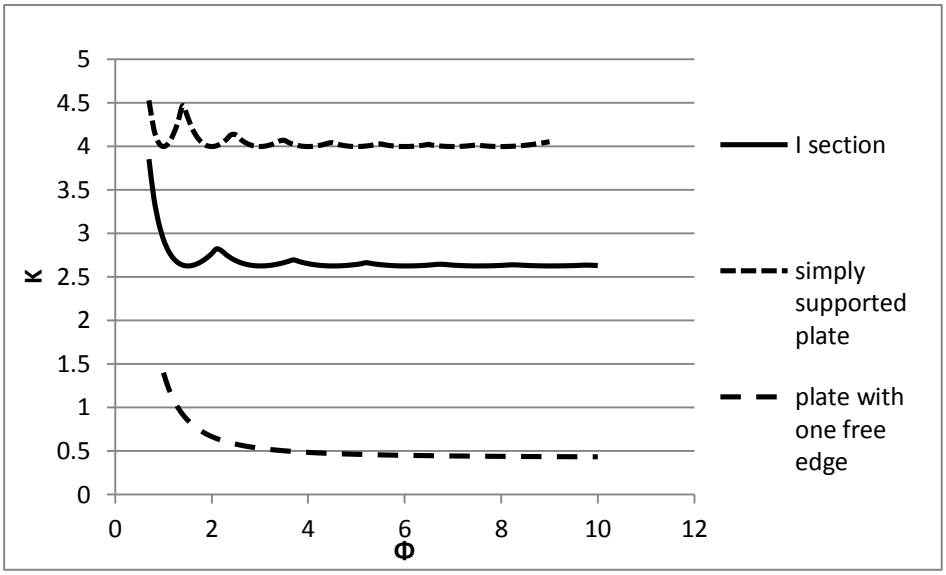

Figure 2.14: Curve K – Φ for I section with b2/b1=0. 5.

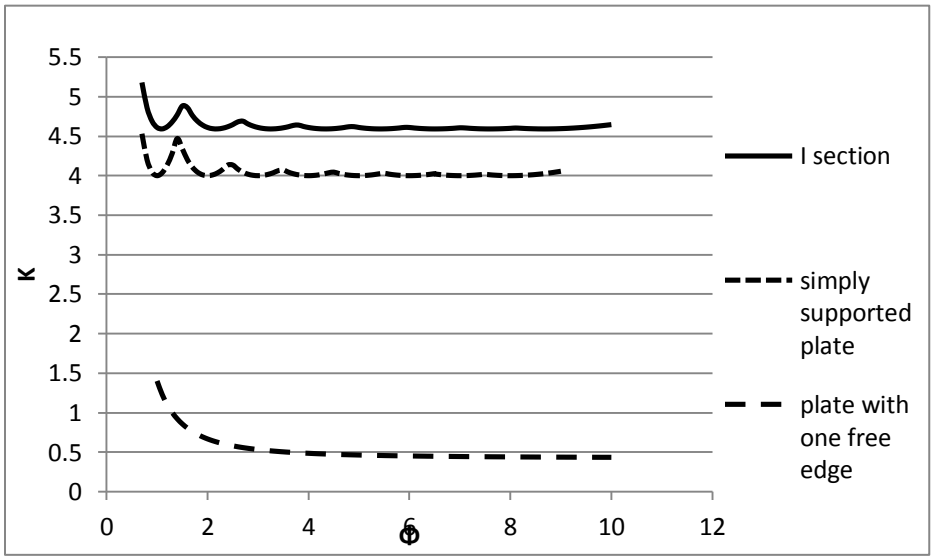

Figure 2.15: Curve K – Φ for I section with b2/b1=0. 3.

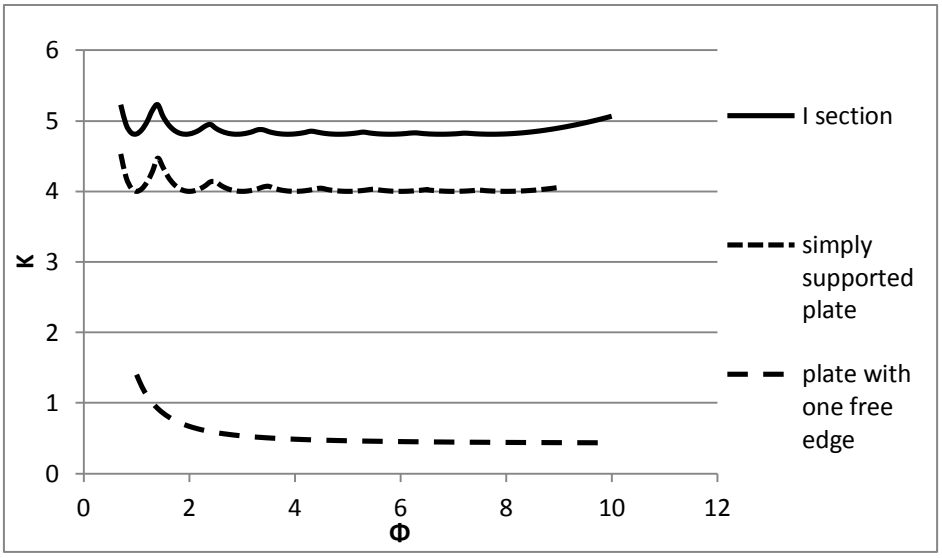

Figure 2.16: Curve K – Φ for I section with b2/b1=0. 1.

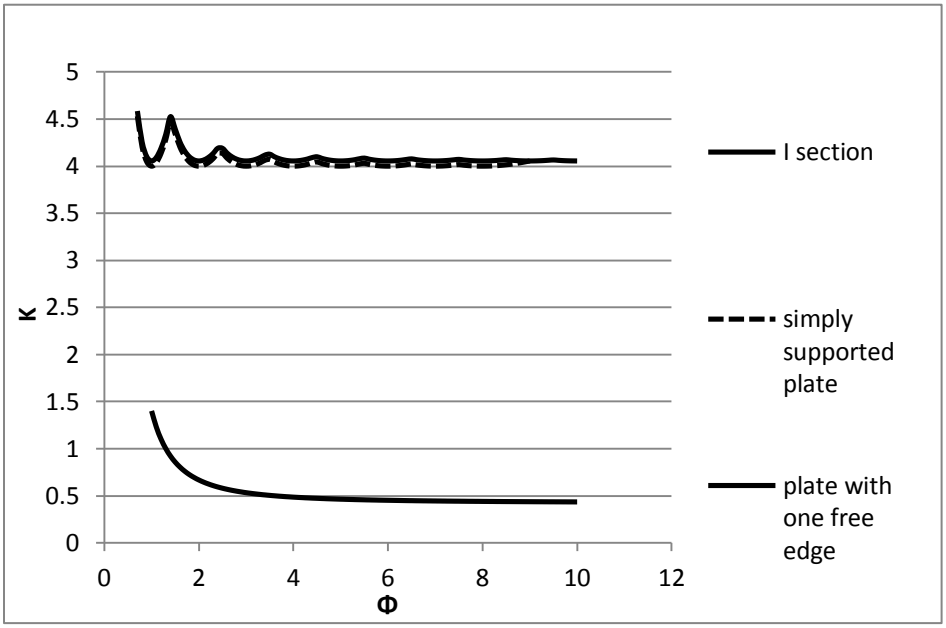

Figure 2.17: Curve K – Φ for I section with b2/b1=0. 005.

In fact, the values of K exceed four, as it can be observed from Figure 2.15, Figure 2.16 and Figure 2.17. Although the cross-section has a very small flange, this small flange instead of turning the web of the I-section into a simply supported plate, can behave as a stiffener of the web causing a stiffness at the edges of the web. The stiffness of the small flanges can therefore increase the parameter K over the value referenced for a simply supported plate.

That behavior of the flange acting as a stiffener was observed for a limited range of the flange's width. For smaller widths, the web becomes a simply supported plate as it's possible to see in the Figure 2.17.

The flange behaving as a stiffener of the web may be explained due to the flange's buckling load. Being the flange so small compared to the web, when comparing the web's and the flange's buckling loads in separate, the lowest buckling load will belong to the web. Therefore, the plate governing local buckling will be the web having at the same time the flanges behaving as stiffeners, explaining the increase of the local buckling load of the I-section over the upper limit defined by the simply supported plate. For bigger widths of the flange, the flange's local buckling load will diminish to a point that the flange will govern buckling of the I-section and the solution for the I-section will be as expected.

Figure 2.18 gives a better perspective of the range where the flanges work as a stiffener of the web. Both plates have the same thickness and length.

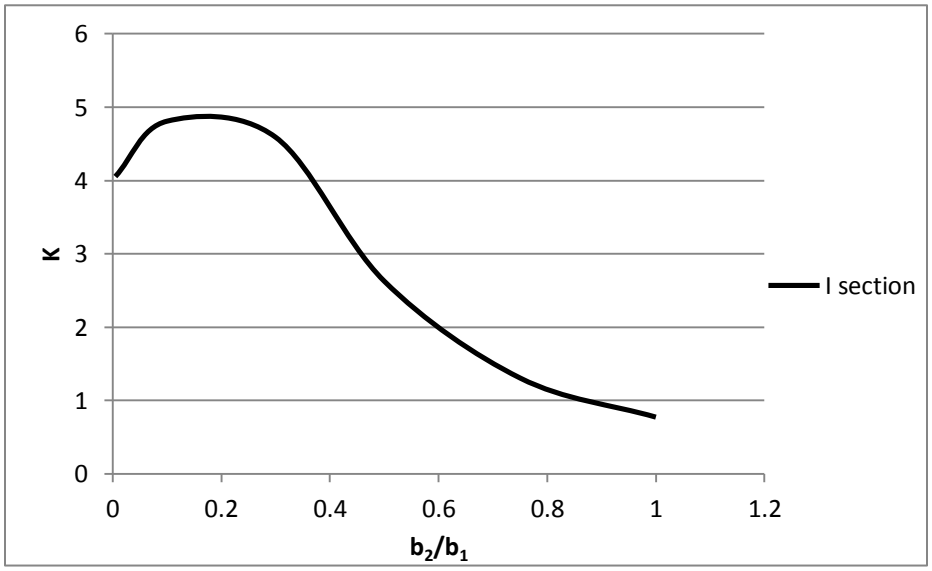

Figure 2.18: Minimum value of K for an I-section with variation of the relation between web and flange width.

2.2.3 Post-buckling of plates

The background theory of post-buckling of thin plates was developed by von Kármán. The assumptions made by von Kármán (Bloom & Coffin, 1944) to derive the nonlinear plate equations are:

(i) The nonlinear terms of the membrane deformations are kept along with the assumptions made in the linear theory of thin plates;
(ii) A linear relation for the bending strains;
(iii) The equilibrium equation relates the stress tensor to the external loading.

The equation of equilibrium (2.60) also stated at the beginning of chapter 2.2.1, follows:

$$\nabla^4 w = \frac{1}{D} * \left(q + N_x \frac{\partial^2 w}{\partial x^2} + 2N_{xy} \frac{\partial^2 w}{\partial x \partial y} + N_y \frac{\partial^2 w}{\partial y^2} \right) \tag{2.60}$$

The assumption of small displacements is no longer valid for the post-buckling analysis of thin-walled section and therefore all terms with higher orders of the displacement field (u, v, w) can no longer be neglected. The membrane deformations are defined as:

$$\begin{cases} \varepsilon_x = u_x + \frac{1}{2} w_x^2 \\ \varepsilon_y = v_y + \frac{1}{2} w_y^2 \\ \varepsilon_{xy} = \frac{1}{2}(u_x + v_y + w_x w_y) \end{cases} \tag{2.61}$$

Being the bending strains given by:

$$\begin{cases} \kappa_{xx} = -w_{xx} \\ \kappa_{yy} = -w_{yy} \\ \kappa_{xy} = -w_{xy} \end{cases} \tag{2.62}$$

Notice that the subscript of the displacement field represents partial derivatives ($w_x = \frac{\partial w}{\partial x}$ for example).

Considering the definitions given in equations ((2.61)-(2.62)) and applying the constitutive relation: membrane forces (equation (2.63)) and bending moments (equation (2.64)) are defined as:

$$\begin{cases} N_x = C(\varepsilon_x + \nu\varepsilon_y) \\ N_y = C(\varepsilon_y + \nu\varepsilon_x) \\ N_{xy} = C(1-\upsilon)\varepsilon_{xy} \end{cases} \tag{2.63}$$

$$\begin{cases} m_{xx} = D(\kappa_{xx} + \nu\kappa_{yy}) \\ m_{yy} = D(\nu\kappa_{xx} + \kappa_{yy}) \\ m_{xy} = D(1-\nu)\kappa_{xy} \end{cases} \tag{2.64}$$

Where C is the axial stiffness of a plate (equation (2.65)) and D is the flexural stiffness (equation (2.7)) described at the beginning of chapter 2.2.1.

$$C = \frac{Et}{1-\upsilon} \tag{2.65}$$

By relating equations (2.64) and (2.65), the compatibility equation can be written as the following equation:

$$\varepsilon_{x,yy} + \varepsilon_{y,xx} - 2\varepsilon_{xy,xy} = w_{xy}^2 - w_{xx}w_{yy} \tag{2.66}$$

By referring the stresses as a stress function F:

$$\begin{cases} F_{yy} = N_x \\ F_{xx} = N_y \\ F_{xy} = -N_{xy} \end{cases} \tag{2.67}$$

The compatibility equation changes to a function of the vertical displacement w and the stress function F.

So the von Kármán equations regarding equilibrium and compatibility of thin plates are:

$$D\nabla^4 w - \left(F_{yy}w_{xx} - 2F_{xy}w_{xy} + F_{xx}w_{yy}\right) = q \tag{2.68}$$

$$\nabla^4 F = Et\left(w_{xy}^2 - w_{xx}w_{yy}\right) \tag{2.69}$$

These equations can also be adopted when the plate has geometrical imperfections. Those imperfections are taken into account as an initial displacement field (u^0, v^0, w^0). Therefore the von

Kármán equations for equilibrium and compatibility for thin plates with geometrical imperfections can be written as:

$$D\nabla^4 w - \left(F_{yy}(w_{xx} + w_{xx}^0) - 2F_{xy}\left(w_{xy} + w_{xy}^0\right) + F_{xx}\left(w_{yy} + w_{yy}^0\right)\right) = q \tag{2.70}$$

$$\nabla^4 F = Et\left(w_{xy}^2 - w_{xx}w_{yy} + 2w_{xy}^0 w_{xy} - w_{xx}^0 w_{yy} - w_{yy}^0 w_{xx}\right) \tag{2.71}$$

2.2.3.1 Simply supported plate

After doing this short summary on post-buckling plate theory, it's time to go back to the first plate example: the simply supported plate with compressive forces in only one direction.

Admitting that the plate is long enough $(a > 4b)$ and applying the equations derived in the section 2.2.3, the equation for a perfect plate can be written as follows:

$$\frac{\sigma}{\sigma_{cr}} = 1 + \frac{3}{8}(1 - \upsilon^2)^2 \left(\frac{q}{t}\right)^2 \tag{2.72}$$

where σ_{cr} is the buckling stress obtained from equation (2.25) and q is the maximum transverse displacement of the plate. If the plate has initial imperfections the equation changes to:

$$\frac{\sigma}{\sigma_{cr}} = \left[1 + \frac{3}{8}(1 - \upsilon^2)^2(\bar{q}^2 + 3\bar{q}\varepsilon)\ \right]\frac{\bar{q}}{\bar{q} + \varepsilon} \tag{2.73}$$

where ε is a parameter related to the initial imperfections and $\bar{q}$ is the amplitude of the deflection normalized in relation to the plate's thickness.

The post-buckling path of a perfect plate and a plate with initial geometric imperfections is represented in Figure 2.19, being possible to verify the increase of the plate's local capacity. The characteristics of the plate are in the Table 2.2.

Table 2.2: Material and geometric properties of the plate.

E (MPa)	210000
v	0.30
b (m)	1.20
a (m)	1.20
t (m)	0.01
σ_{cr} (MPa)	52.72

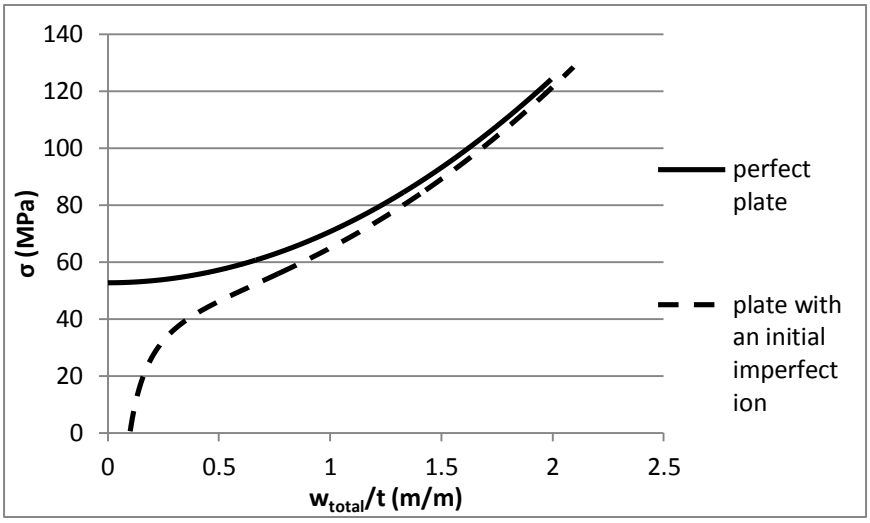

Figure 2.19: Post-buckling of a square plate.

$w_{total}/_{t}$ is the total and maximum transverse displacement of the column normalized by the plate's thickness.

The increase of the resistance of a plate due to post-buckling is due to the appearance of tension in the transverse direction for which the buckling occurs. After buckling, in the edges where the load is applied, the stresses have a nonlinear distribution. In the other direction, some tension stresses will appear to restore equilibrium and are the reason for the increase of the load capacity in post-buckling of plates.

To accommodate the nonlinear distribution of stresses along the edges and its impact on the plate's resistance, the concept of effective width was suggested by von Kármán *et al* (von Kármán, Sechler, & Donnell, 1932) and it will be very useful when dealing with the Eurocodes and calculating the load resistance of plates. The concept of effective width allows the changing of the real distribution of stresses, along the width's plate, that are nonlinear to a width which has a uniform distribution of stresses. That effective width has a uniform stress distribution and it is statically equivalent to the real width of the plate.

3. Finite element model

A finite element (FE) model was adopted for the stability analysis of thin-walled structures.

The FE models will also be used to compare the theoretical formulations written in the previous chapter. Two types of examples were analyzed: a simply supported plate and an I-column.

The simply supported plate was analyzed because it was the simplest example. Being a simple example, it was possible to model it with the finite elements and evaluating its local buckling load and the local post-buckling behavior. Concerning the I-column, there is no theoretical formulations to be compare with the numerical results for the local post-buckling behavior. Therefore, modeling a simply supported plate was helpful to model the I-column because the same modeling principles used in the simply supported plate were applied to the column.

3.1 Finite element program

The FE model was implemented in the commercial software Abaqus 6.13, being a well-known software, all the theory used and all the explanations are presented in Abaqus's library (Abaqus 6.13 Documentation).

The Abaqus software was mainly used to evaluate buckling loads of the examples and to compute the corresponding post-buckling paths as well as the entire combined trajectory of load-displacement field of the examples with nonlinear geometrical behavior.

To obtain the buckling loads, Abaqus has a function called "BUCKLE". It's an eigenvalue buckling analysis used to estimate the critical (bifurcation) load of structures. The function tries to determine "the loads for which the model stiffness matrix becomes singular" (Abaqus 6.13 Documentation). At the end of the buckling analysis the function returns as an output the corresponding values of the eigenvalues.

The other function adopted was the "STATIC" function. It's a function that provides static stress/displacement analysis with a static load step. This static analysis is used for obtaining the load-displacement field starting from the unloaded condition to the post-buckling domain. To make this analysis possible, the Riks method was used.

The Riks method is adopted given the non-linear geometrical behavior of the structure. The method uses a load-deflection analysis to determine the post-buckling path of the structure. Riks method

uses a relation based on the arc length. This approach provides solutions regardless of whether the response is stable or unstable. More information about the Riks method can be found at the Abaqus's manual (Abaqus 6.13 Documentation).

As the software's manual indicates, in order to use the Riks method to perform a post-buckling analysis it's necessary to introduce an initial geometric imperfection into the "perfect geometry" of the structure at study to turn the structure's behavior "(…) into a problem with continuous response instead of bifurcation" (Abaqus 6.13 Documentation).

So those initial geometric imperfections were introduced by considering the "IMPERFECTION" function. The imperfections are added in the "perfect" structure by adding the scaled buckling in order to create the perturbed mesh. The imperfections adopted are defined in Eurocode 3. Therefore, the imperfections were derived from the buckling shapes of the global buckling and the local buckling modes with the magnitudes evaluated accordingly to the Eurocode 3 and explained in section 4.2.

All the examples studied were written in an input file that was ran by the software and after that all the results were analyzed in order to verify the goal of this thesis: the interaction between local and global buckling modes. The examples were all modeled with shell elements S4R.

Element S4R is a standard large-strain shell element with "4-node general-purpose shell, finite membrane strains" (Abaqus 6.13 Documentation). It has six degrees of freedom per node: three translations and three rotations. It also has a uniformly reduced integration to avoid shear and membrane locking. It also converges to a shear flexible theory for thick shells and to a classical theory for thin shells. Hence, it can be concluded that the element chosen is a suitable element for the buckling analysis of thin-walled structures.

3.2 Finite element mesh

An adequate mesh of the structures is very important when dealing with finite element method analysis. If a mesh is too coarse, the results obtained from the analysis may not be sufficiently accurate. On the other hand, if a mesh is too refined, the analysis can develop accurate results but it'll increase the processing time with computational costs. This affirmation can be supported by section 4.1.1, Figure 4.1 where a comparison between the theoretical and the finite element results was performed.

So, in order to have the most accurate results without spending too much processing time, it was decided to model all the structures with a reasonable mesh. That was obtained by running several convergence studies. The mesh will of course be different whether the study is related to a single plate or an I-column.

For a simply supported plate, the finite element mesh adopted is shown in Figure 3.1.

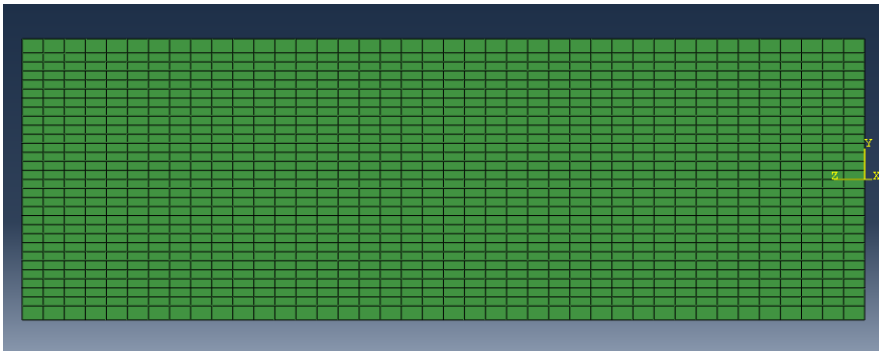

Figure 3.1: Typical finite element mesh for a simply supported plate.

About the mesh of the I-section column, the flanges were modeled with 10 elements along its width and the web has 20 elements across its height. The typical finite element mesh for a column is shown in Figure 3.2. For the single plate and the I-column, the structure was divided in seventy equal sections along the axial axis. This gives a reasonable mesh for a wide range of lengths. An analysis, present in the subchapter 4.1.2 was also performed to compare the numerical and the theoretical results for an example of a column.

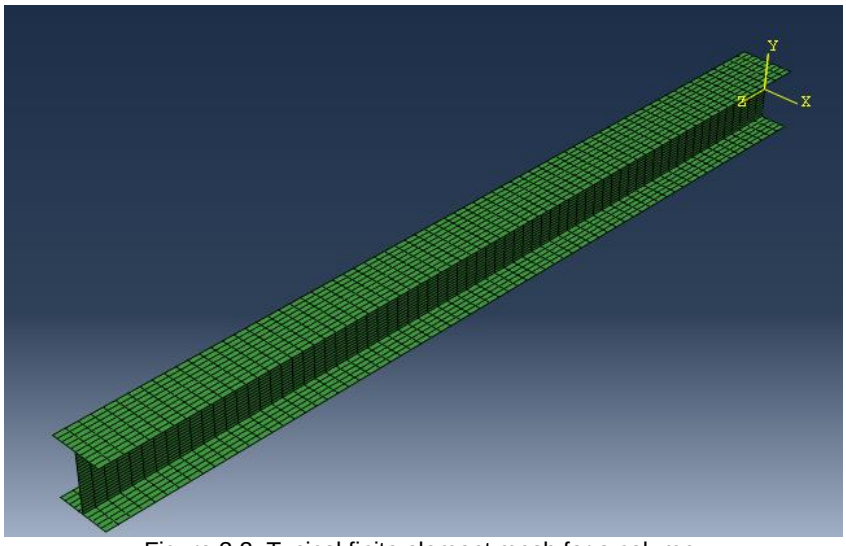

Figure 3.2: Typical finite element mesh for a column.

3.3 Geometric and material properties

The main objective of this thesis is to perform a nonlinear finite element analysis of two types of structures: simply supported plates and I section columns.

The properties that define the dimensions of the plates will be given in chapter 4. However it's important to state that single plates have the same thickness t over the length a, being the cross section's height defined by b.

About the columns (Figure 3.3), the upper flange and the lower flange have the same t_f thickness, the same width b and length L. The web is defined by its height h and it has a thickness t_w.

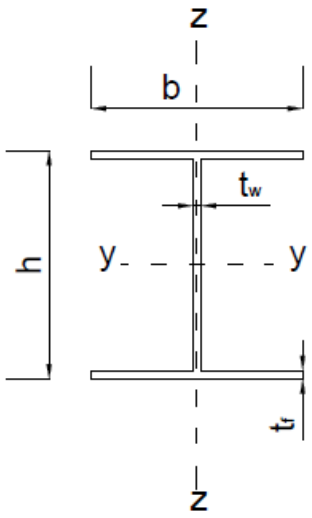

Figure 3.3: Cross-section of the I-column.

The material adopted was the steel of grade S355, being the relevant information about this material shown in the following table.

Table 3.1: Material properties of steel S355.

Material	S355
Young's modulus (N/mm^2)	210000
Poisson's ratio	0.3
σ_y (N/mm^2)	355

The material was considered as being elastic perfectly plastic and the Abaqus software considers the Von Mises stresses to verify yielding.

3.4 Initial geometric imperfections

The Eurocode 3 defines the geometric imperfections of the structures. That is due to the fact that a real structure is never flat and without imperfections and therefore it's necessary "to cover the effects of imperfections, including residual stresses and geometrical imperfections such as lack of verticality, lack of straightness, lack of flatness (…) " (EN 1993-1-1:2005).

The Eurocode also states that those initial geometric imperfections can be treated as buckling shape modes. Thus, depending on the structure at study, its geometric imperfections are derived from the first buckling mode with a specific magnitude specified by the Eurocode 3. Therefore, the imperfections are introduced in the initial and perfect shape of the structure by adding the nodal displacement from the scaled buckling shape mode (by using the imperfections' amplitudes) to the initial shape of the structure.

For the single plates, the only geometric imperfections are derived from local buckling, whereas for the columns, three different geometric imperfections were considered: two regarding the bending axis and one the local buckling mode. The amplitude corresponding to local modes is given by the width of the web because, in this thesis's examples, it is the web that governs local buckling.

The amplitudes of global buckling modes are related to the buckling length. The examples used in this thesis have in both ends of the column, the rotation around the minor axis fixed. This means that the buckling length is not the column's length but only half of it.

Finally, and according to the Eurocode 3, the global imperfection around the minor axis was defined as being the leading imperfection, being the imperfection associated with the other global buckling mode and the local buckling mode defined as being the accompanying imperfections which "(…) may have their values reduced to 70%." (EN 1993-1-5:2006).

3.5 Boundary and load conditions

Boundary conditions are very important when modeling a structure by finite element model. It took a lot of time to successfully obtain the appropriate boundary conditions and constraints in order to model all possible buckling modes.

For the single simply supported plate, the boundary conditions used to model the theoretical plate were:

- All the nodes at the extremities have their horizontal (y-axis) displacement fixed.
- The middle nodes at the edges (points A of the Figure 3.4) have their vertical (z-axis) displacement fixed in order to the other nodes to be able to deform by the Poisson's effect.
- The node alignments at the top and bottom (z-direction) of the plate have their horizontal (y-axis) displacements and rotation around the vertical axis (z-axis) fixed in order to have only local buckling shapes.
- Also the middle node of the plate has its longitudinal displacement (x-axis) fixed.

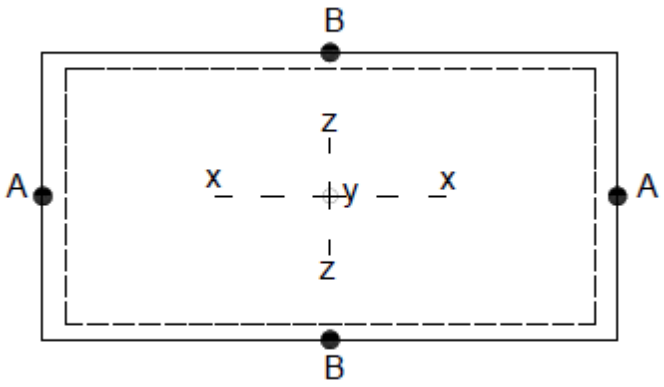

Figure 3.4: Simply supported plate with the axis orientations.

These boundary conditions were defined in order to obtain the eigenvalues of the buckling analysis and the buckling modes. To perform a post-buckling analysis, as it was stated in section 2.2.3.1, that the longitudinal edges (edges which contain point B in Figure 3.4) needed to have the same displacement so all the nodes have the vertical displacement (z-axis) and longitudinal displacement (x-axis) related to the middle nodes (nodes B) of the alignments. By doing that it was possible to keep the node alignments straight.

The same procedure for the columns was applied because they all are simply supported structures at least in one direction. In the minor axis, the rotation was fixed in order to have half of the buckling length compared to the other direction.

For these structures, it was necessary to have global and local buckling modes in separate models.

Regarding global buckling, it was necessary to model its cross-sections to act as a rigid body and at the same time it was important to ensure buckling over both cross-sectional axes. So accordingly to what was defined, the cross-sectional nodes and its degrees of freedom were constrained with

kinematic coupling constraints to the middle node (master node: point A from Figure 3.5) along the column.

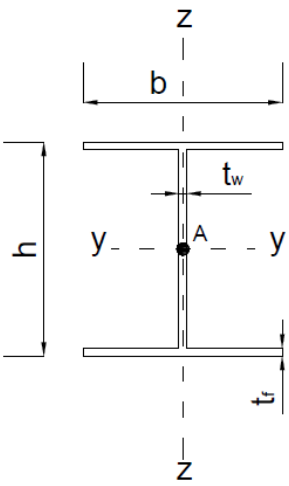

Figure 3.5: Cross-sections with the master node.

From Abaqus' library (Abaqus 6.13 Documentation), the definition of kinematic coupling is: "it constrains the motion of the coupling nodes to the rigid body motion of the reference node. The constraint can be applied to user-specified degrees of freedom at the coupling nodes with respect to the global or a local coordinate system. (…) Kinematic constraints are imposed by eliminating degrees of freedom at the coupling nodes (…)". So by changing those degrees of freedom that were constrained it was possible to compel over which axis the buckling occurs.

Regarding the boundary conditions to obtain buckling over the minor axis, the column needs to have the column's ends fixed on the middle node (point A of Figure 3.5) so the cross-section can't move on its cross-sectional plane neither it can't rotate around z-axis. The mid node alignment (starting in point A, Figure 3.5, from one end of the column to the other) is vertically (z-axis) fixed and it can't rotate on its cross-sectional plane and finally the column's middle node can't have longitudinally (x-axis) displacements.

To obtain buckling over the major axis, the boundary conditions have only slightly changes from the previous buckling axis. It has the same boundary conditions on the column's ends but now, in order to enforce buckling over the major axis it was necessary to impose zero displacements (y-axis) on the middle node alignment (from point A, Figure 3.5, of one end to the other) as well as on the top and bottom alignments. Moreover, the torsional rotation is fixed along the column's length.

To have a model with just local buckling, it was necessary to prevent any form of global buckling. So torsion was prevented, vertical (z-axis) displacements of the cross-sections extremities were set to zero as well as the horizontal (y-axis) displacement. Then the top and bottom node alignments

were prevented from having horizontal (y-axis) displacements and the middle node alignment was prevented from having vertical (z-axis) displacements. Finally, the flanges at the extremities of the structure were set to have a rigid body motion.

All written above is to have a specific buckling mode in order to study all buckling modes separately. To study the interaction of modes, no constraints along the column were used. So, with the necessary boundary conditions it was possible to have a model in which, depending on the length of the structure, the “true behavior” of the column would be evaluated. This means that buckling will depend on the slenderness of the structure. For a column with a lower slenderness, local buckling has the lowest buckling load, whereas for a higher slenderness column, global buckling is the governing phenomenon. For a small range of lengths, there will be an interaction between local and global buckling modes.

Concerning load conditions, all loads applied on the structures were model as nodal forces applied at the end cross-sections. Either for a plate or a column, the uniform compression load was applied through nodal forces according to the geometric properties of the structure.

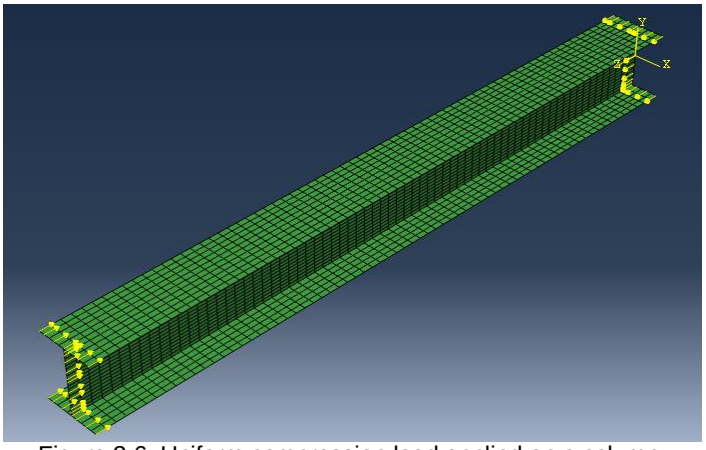

Figure 3.6: Uniform compression load applied on a column.

4. Results

This section presents all the results obtained from the finite element method analysis performed by Abaqus software, which are compared with the theoretical results. It also has the general guidance given by the EC3 to evaluate the design buckling resistance of a compression member.

It is divided into three different sections: the first one with the validation of the finite element models for the two structures that were studied across this thesis: simply supported plates and simply supported columns; the second section that explains the guidelines given by the EC3 to obtain the design buckling resistance of a compressed member; and the last section is for the results from the interaction between buckling modes performed by the FE analyses.

Notice that it will be in this chapter that interaction between buckling modes will be studied but it is important to understand that there's no theoretical formulas available for the interaction of buckling modes for an I-section so the numerical results can only be trusted with a certain level of confidence.

4.1 Validation of the FE models

4.1.1 Simply supported plate

Single plates were only studied in order to have a starting point to a more complex problem: the buckling analysis of thin-walled I-columns.

Regarding the affirmation done in section 3.2 about the finite element mesh of a single plate, an analysis of simply supported plate demonstrates that the mesh chosen to model the structures gives accurate results for a big range of the plate's lengths.

Figure 4.1 shows the accuracy regarding the finite element method model in comparison to the equation (2.25) that is used to calculate the buckling load.

The material and geometric properties of the plate loaded in one direction with compressive forces are given in Table 4.1.

Table 4.1: Material and geometric properties of the simply supported plate

E (MPa)	210000
v	0.3
b (m)	1.2
t (m)	0.01

In Figure 4.1 the results obtained from the model are compared with the corresponding results from the formula (equation (2.25), section 2.2.2.1).

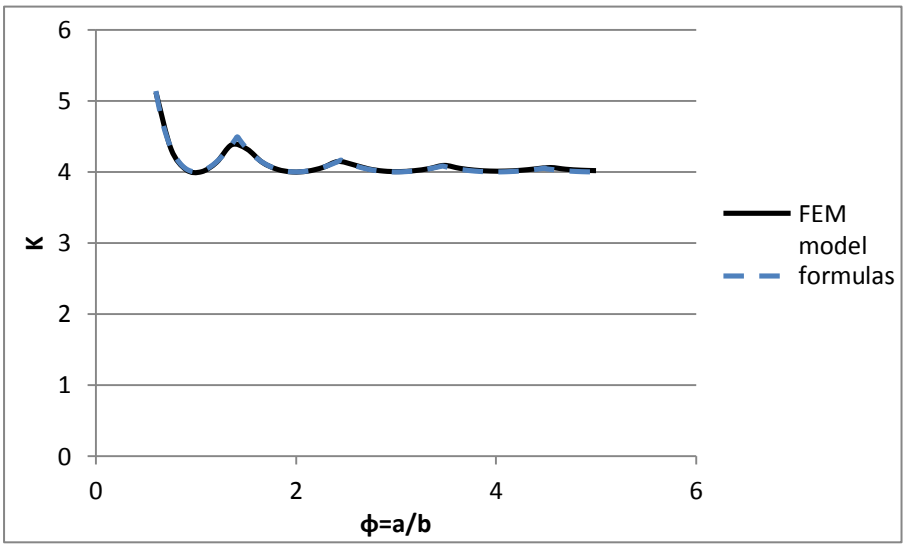

Figure 4.1: Comparison of results from the finite element model and the theoretical equations form the critical buckling load of a simply supported plate loaded in one direction.

The model can accurately evaluate the buckling load of a simply supported plate, being the results in an excellent agreement with the results obtained from the application of formula (2.25) in section 2.2.2.1.

The post-buckling behavior of the simply supported plate obtained from the finite element model was also successfully compared with the results obtained from equation (2.72) (section 2.2.3.1). The results are represented in Figure 4.2. The model corresponding to the post-buckling analysis has the material and geometric properties as defined in Table 4.1. A long plate with $a > 4b$ was considered.

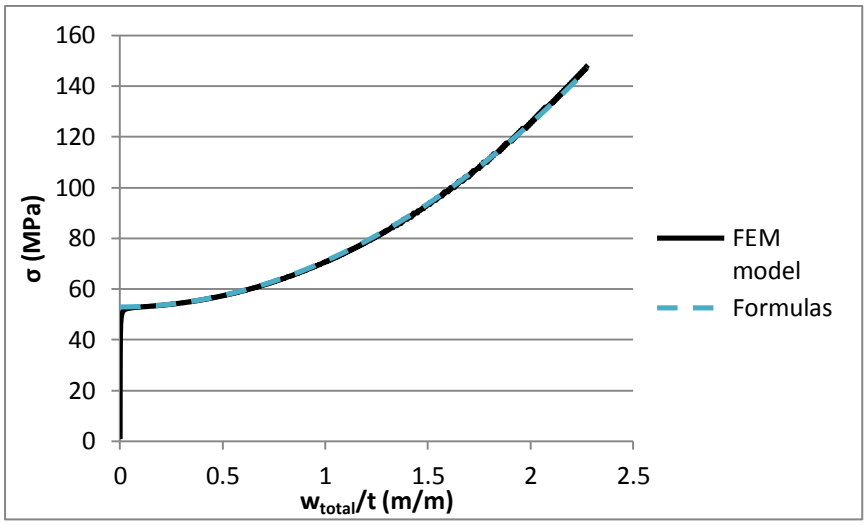

Figure 4.2: Comparison of results from the finite element model and the theoretical equations for a simply supported plate uniformly compressed in one direction.

It's possible to verify that both results (numerical and analytical) are quite similar. So the finite element model of a simply supported plate complies with its purpose, being therefore adopted in this study and it will be use from now on.

4.1.2 I-Column

A validation of the finite element model for the buckling analysis of columns is presented in this section. A column with an I shaped cross-section with the characteristics given in Table 4.2 is considered.

Table 4.2: Example of a column used to validate the finite element models.

L (m)	29.5
h (m)	3
b (m)	1.8
t_w (m)	0.06
t_f (m)	0.06

Being h the web's height and $t_w$the web's thickness. b is the flange's width and t_f is the flange's thickness. The cross-sectional properties are also defined in Figure 4.3.

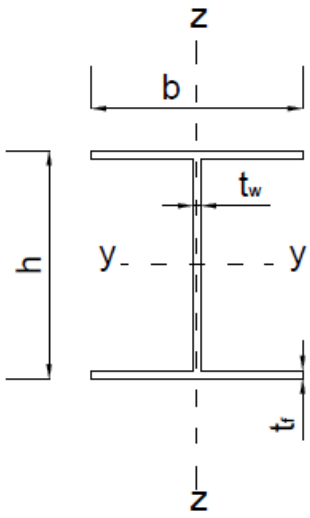

Figure 4.3: I shaped cross-section.

The local buckling results will be compared with the results obtained in section 2.2.2.3 for this particular column (Table 4.2). Regarding local buckling, the critical stresses corresponding to local buckling were obtained from the FE model and from equations (2.50)-(2.57) in section 2.2.2.3, being given in Table 4.3. Unfortunately, there are no theoretical equations regarding local post-buckling to compare the results from the finite element model.

Table 4.3 presents the difference between the critical stress from the finite element model and the stress obtained from the equations.

Table 4.3: Comparison of local buckling results between the FE model and the theoretical equations for a column.

Local buckling	
k_{theory}	4.592
$k_{FE\ Model}$	4.639
$\sigma_{cr,local,theory}$ **(MPa)**	348.589
$\sigma_{cr,local,FE\ Model}$ **(MPa)**	352.166
Error (%)	1.016

The results show the difference between the finite element model and the theoretical equations with an absolute error difference of about 1%.

The local buckling mode is represented in Figure 4.4. The mode has several equal half-waves, being the deformed shape similar to the one defined when deriving the buckling equations in chapter 2.2.2.3.

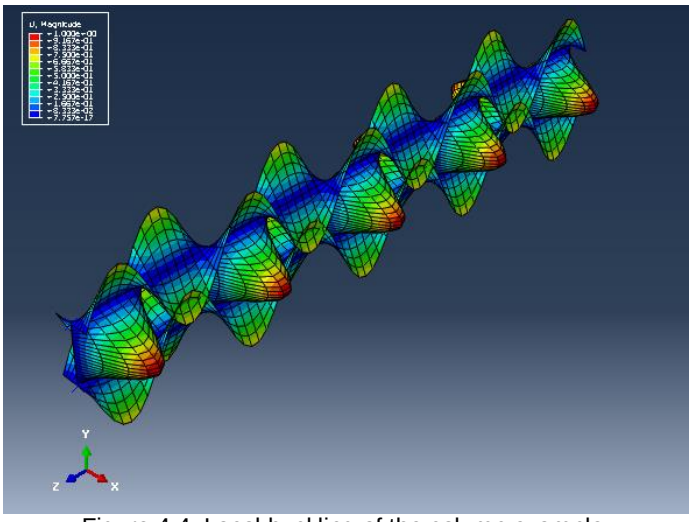

Figure 4.4: Local buckling of the column example.

The post-buckling path obtained from the model is represented in Figure 4.5, being possible to observe that the load has a stable path increasing the strength after buckling.

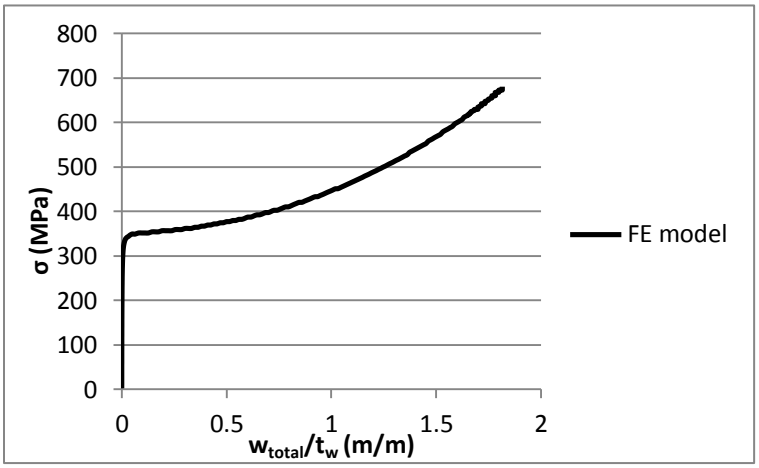

Figure 4.5: Local post-buckling results from the finite element model for a simply supported column uniformly compressed.

Notice that the stress ($\sigma = \frac{P}{A}$) is the stress applied in the column and the displacement is the horizontal displacement of the middle of the column as represented in Figure 4.6.

Global buckling and post-buckling results from the FE model will be compared with equation (2.1) and equation (2.2) from section 2.1.

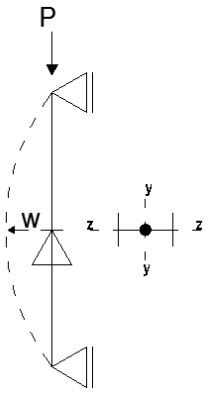

Figure 4.6: Applied load on the simply supported column and the corresponding displacement.

The critical stresses corresponding to global buckling are given in Table 4.4, being the absolute error difference almost 2%

Table 4.4: Comparison of global buckling results between the FE model and the theoretical equations for a column.

Global buckling	
$\sigma_{cr,global,theory}$ (MPa)	354.282
$\sigma_{cr,global,FE\ Model}$ (MPa)	348.981
Error (%)	1.519

The post-buckling path of the column obtained from the FE model and according with the post-buckling theory is represented in Figure 4.7. Notice that in a column, the post-buckling behavior is stable with a slightly increase of the column's strength.

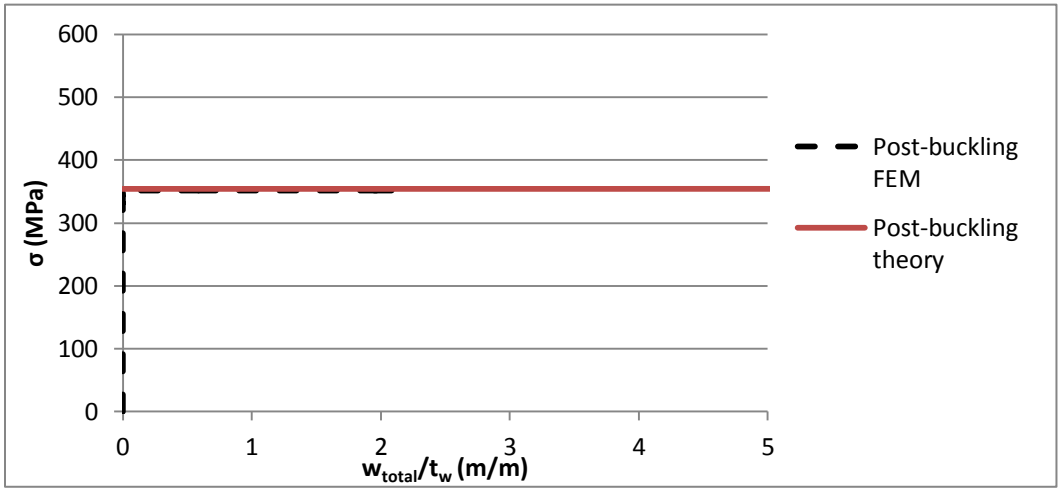

Figure 4.7: Comparison of the global post-buckling results from the finite element model and the theoretical equations for a simply supported column uniformly compressed.

Both local and global buckling results and the corresponding post-buckling behavior obtained from the FE model have small differences relatively to the available theoretical equations. Therefore the FE model is considered valid for the purposes of this thesis that is the study of the interaction between local and global buckling modes of a thin-walled steel column.

4.2 Eurocode 3

The Eurocode that gives guidance to deal with steel structures is the Eurocode 3 (EC3) (EN 1993-1-1:2005). Since this present thesis is focused on buckling of thin-walled steel structures, all the necessary information addressed about buckling of thin-walled columns in the EC3 will be examined.

It is known that the steel elements used have always imperfections so they need to be taken into account “to cover the effects of imperfections, including residual stresses and geometrical imperfections such as lack of verticality, lack of straightness, lack of flatness (…) “ (EN 1993-1-1:2005).

Those imperfections can be related to global imperfections for overall elements or local imperfections for individually members.

For global imperfections the EC3 (EN 1993-1-1:2005) recommends imperfections that are given in table 5.1 (elastic analysis) of the Eurocode where a design value for the global imperfection according to the buckling length of the element is given. That table is related to table 6.2 of the same Eurocode and it defines the buckling curve for a cross-section of uniform members in compression.

Regarding local imperfections, it is a different section of the EC3 (EN 1993-1-5:2006) that gives recommendations about the values of the local imperfections to be adopted in an analysis performed by finite elements. Recommendation concerning local imperfections is given by table C.2 where equivalent geometrical imperfections are proposed concerning local and global imperfections. The local type of imperfection chosen uses the buckling shape as an imperfection. Notice that the global imperfections that are recommended are referred to the table 5.1 that was described above.

These two types of imperfections proposed by the Eurocode, global and local imperfections, will be adopted for a stability analysis through a finite element model.

However, the EC3 (EN 1993-1-5:2006) defines that “in combining imperfections a leading imperfection should be chosen and the accompanying imperfections may have their values reduced to 70%.” It is also stated that any type of imperfections can be choose for leading imperfection. In this case the global imperfection for the minor global axis was chosen as the leading imperfection so the amplitude of the local buckling mode and the amplitude of the other global axis are reduced to 70% of its value.

Now a short summary of the classification of cross-sections will be done because cross-sections have a great impact on local buckling due to its small thickness.

Chapter 5.5 and more specifically table 5.2 of the EC3 (EN 1993-1-1:2005) describes the classification of cross-section and defines Class 4 cross-sections as the ones prone to local buckling because these type of cross sections “are those in which local buckling will occur before the attainment of yield stress in one or more parts of the cross-section.”

Notice that the EC3 also states that a “cross-section is classified according to the highest (least favorable) class of its compression parts (…)”. This sentence will relevant when analyzing the uniform compression because it will be important to have different classifications between the web and the flanges.

Since cross-sections of class 4 are prone to local buckling, it is possible to study local buckling before yielding therefore it gives the possibility to study the interaction between global and local buckling modes.

The same part of the EC3 also allows the use of the concept of effective width developed by von Kármán (von Kármán, Sechler, & Donnell, 1932) in Class 4 cross sections to take into account the “(…) reductions in resistance due to the effects of local buckling (…)”.

The EC3 uses the effective width to calculate the design buckling resistance of compression members of class 4 cross-sections (EN 1993-1-5:2006). For the other classes, the effective width is not used.

So by applying equation 6.47 or 6.48 of the EC3 (EN 1993-1-1:2005) it is possible to calculate the design buckling resistance of a column.

Therefore the design buckling resistance given by the EC3 will be used further in this thesis to compare the ultimate load capacity from the results of the finite element method. The ultimate load capacity from the FEM analysis is obtained considering the maximum load of the load path and not the load from which the structures starts to yield. EC3 (EN 1993-1-5:2006) in Annex C states that

“for structures susceptible to buckling” the ultimate limit state criteria should be focused on the maximum load when a finite element analysis is performed.

4.3 Results from the interaction between local and global buckling modes

The results of the non-linear analysis of the column considering the imperfections defined in the EC3 are presented in this section.

Accordingly to the EC3 (EN 1993-1-5:2006) for structures susceptible to buckling, the ultimate load capacity of the column is defined as being the maximum load therefore this definition of the ultimate load capacity will be applied to the FE results. Therefore it will be considered that the ultimate load capacity of a structure is reached when the structure starts to be unstable as defined in the EC3.

A comparison between the ultimate load capacity of several FE examples and the design buckling resistance from the Eurocode 3 will be performed. That will verify if the EC3 has a conservative approach for the prediction of the design buckling load and if it takes into account the interaction between buckling modes.

Since the beginning of this thesis, the objective was to study the interaction between local and global flexural buckling modes of thin-walled steel structures. For that reason, a cross-section of a column was defined in order to achieve similar buckling loads between the local buckling load and the global buckling loads over the two flexural axes of the column.

Defining a cross-section to achieve similar buckling loads was only possible if the rotation over the minor axis at the column’s ends was not allowed. Fixing the rotations at the ends resulted that the torsional buckling mode became the governing mode and it has a significant impact on the interaction between buckling modes.

Being the objective of this thesis the study of the interaction between local and global flexural buckling modes, the torsional buckling mode was out of the range of the study. Therefore, the FE models were prevented to have torsion and all the results regarding the torsional buckling mode were ignored in order to be possible to study only the interaction between local and global flexural buckling modes, being the global flexural buckling modes, from now on, considered as global buckling modes.

4.3.1 Column

To study the interaction between the local and global buckling modes, a column with the characteristics given in Table 4.5 was defined in order to take into consideration several points:

- Local and global buckling loads should be similar;
- The cross-section should be of class 4;
- In local buckling, the web is the one that governs the buckling mode;
- Local buckling should have odd number of half-waves (when the interaction between local and global buckling modes occurs, the mid-point of the column will have the maximum combined transverse displacement);
- The column has an uniform compression load;

The cross-section of the column is defined in Table 4.5. Notice that the cross-section adopted is not a usual example of a column and all the conclusions that are going to be drawn cannot be directly extrapolated to all types of columns.

Table 4.5: Cross-section of the column.

h (m)	0.95
b (m)	0.85
t_w (m)	0.019
t_f (m)	0.03

To study the interaction between local and global buckling modes, three different examples are going to be analyzed in order to verify the impact of having similar buckling loads for the local and global modes and to study the impact of having interaction between global buckling modes. To do so, one column should have similar buckling loads, another should have lower global buckling loads than the local load and finally the last case should have global loads higher than the local buckling load.

The boundary conditions of the column will be modified in order to ensure similar global buckling modes. The ends of the column are fixed regarding the flexure around the minor axis and pinned at the other direction.

By doing so and by changing the column's length, it will be possible to have the following examples.

- One with similar buckling loads: Case I ($P_{cr,global,z}$= $P_{cr,global,y}$= $P_{cr,local}$);
- One with similar overall buckling loads lower (40% lower) than the local buckling load: Case II ($P_{cr,global,z}$= $P_{cr,global,y}$< $P_{cr,local}$);
- And one with similar overall buckling loads but higher (40% higher) than the local buckling load: Case III ($P_{cr,global,z}$= $P_{cr,global,y}$> $P_{cr,local}$);

Case I ($P_{cr,global,z}$= $P_{cr,global,y}$= $P_{cr,local}$)

Case I ($P_{cr,global,z}$= $P_{cr,global,y}$= $P_{cr,local}$) has a column with similar local and global buckling loads in order to amplify the interaction between the buckling modes.

The length and slenderness of the column are defined in Table 4.6.

Table 4.6: Column's length and slenderness.

L (m)	29.4
$\overline{\lambda_z}$	0.825
$\overline{\lambda_y}$	0.814

The buckling loads of the column are given in Table 4.7.

Table 4.7: Buckling loads.

$P_{cr,local}$ (MN)	31.29
$P_{cr,global,z}$ (MN)	29.14
$P_{cr,global,y}$ (MN)	30.55

Both the web and the flanges are classified according to the EC3 as class 4. The analysis of the web as a simply supported plate has an associated buckling load which is lower than the buckling load of the flange (as a simply supported plate with a free edge). The critical buckling load considering the plate members in separate is given in Table 4.8.

Table 4.8: Critical local buckling stresses of the column and its plated members.

K_{flange}	0.43
$\sigma_{cr,local,flange}$ (MPa)	406.66
K_{web}	4.00
$\sigma_{cr,local,web}$ (MPa)	303.68
K	5.93
$\sigma_{cr,local}$ (MPa)	450.24

Notice that the value of the K parameter when considering the I-section as an assemblage of plates is higher than the value for the simply supported plate because of the fact that the flanges may work as a stiffener to the web. A possible explanation was written in section 2.2.2.3.

The geometric imperfections of the column were defined according to EC3, being the corresponding amplitudes of the buckling shapes given in Table 4.9.

Table 4.9: Amplitudes for the column when Pcr,global,z= Pcr,global,y= Pcr,local.

Amplitudes	
Global buckling shape,z (L/200) (m)	0.1470
Global buckling shape,y (0.7*L/250) (m)	0.0823
Local buckling shape min (h/200; L/200) (m)	0.0033

Notice that the buckling shape mode governing the imperfections is the global buckling mode that corresponds to the flexure about the minor axis, being other imperfections reduced to 70% of the value of their amplitudes.

For Case I ($P_{cr,global,z}$= $P_{cr,global,y}$= $P_{cr,local}$), the local and global buckling modes were analyzed in separate. Figure 4.8 presents the curves “global mode (minor axis)” and “global mode (major axis)” that correspond to the buckling over the minor and major axes respectively and its post-buckling behavior for the column without geometric imperfections. The curve “local mode” represents the local buckling and post-buckling load path for the perfect column.

Notice that Figure 4.8 has the load-displacement relation of the column, being the displacement the maximum transverse displacement of the middle of the column.

Then, the geometric imperfections will be added to the column and a set of models will be created in order to study if having similar buckling loads has any effect on the load-displacement relation.

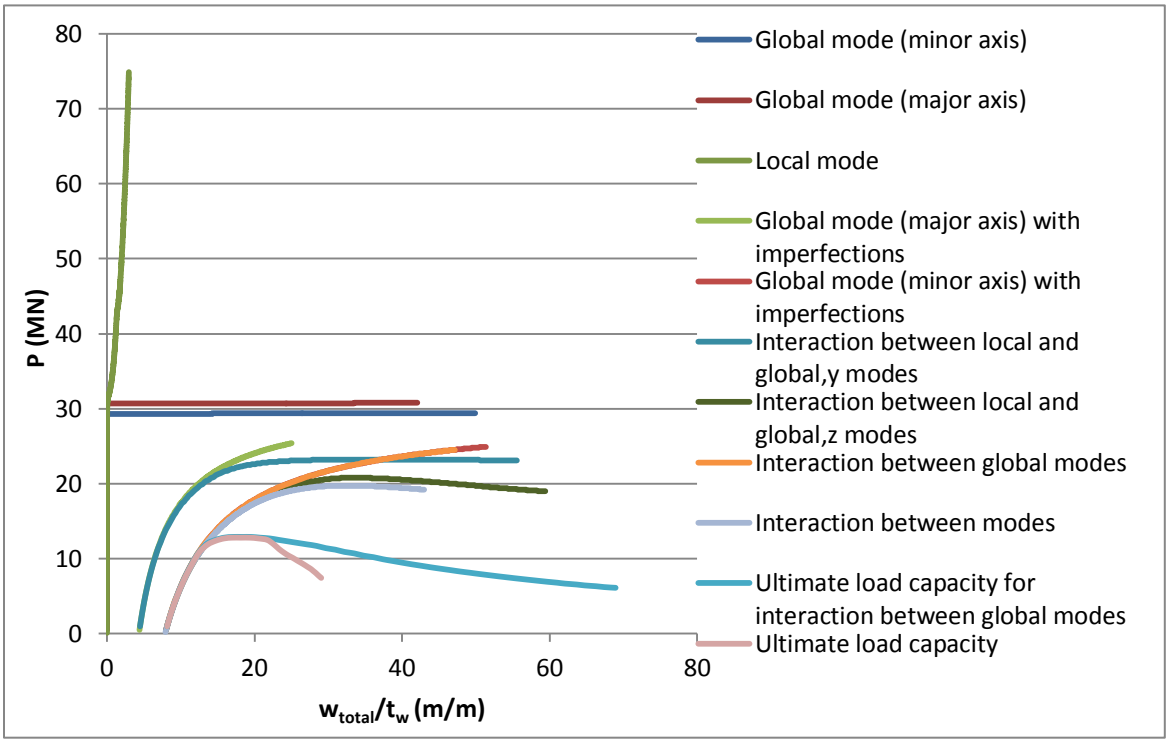

Figure 4.8: Load-displacement for Pcr,global,z= Pcr,global,y= Pcr,local.

The curves “global mode (minor axis) with imperfections” and “global mode (major axis) with imperfections” represented in Figure 4.8, correspond to the buckling mode over the minor and major axes respectively. Both curves consider the imperfections defined in the EC3 and can only deform regarding the corresponding buckling axis, being the in-plane deformations neglected. The curve “local mode” has also the geometric imperfections defined in the EC3 but it has only in-plane deformations, consequently no global buckling occurs.

Figure 4.8 presents also the curves: “interaction between local and global,y modes” and the “interaction between local and global,z modes”, being respectively, the interaction between the local buckling mode with the global buckling mode over the major and minor axis. The FE model used for both curves was allowed to have in-plane deformations along with bending over its buckling axis.

The deformed shape of the column for the curve “interaction between local and global,z modes” and for the curve “interaction between local and global,y modes” are given in Figure 4.9 and Figure 4.10 respectively.

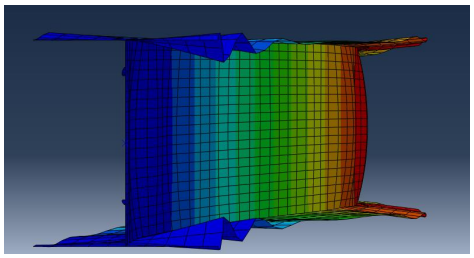

Figure 4.9: Deformed shape of the column when it can only buckle around the z-axis and in-plane deformations are allowed for Pcr,global,z= Pcr,global,y= Pcr,local.

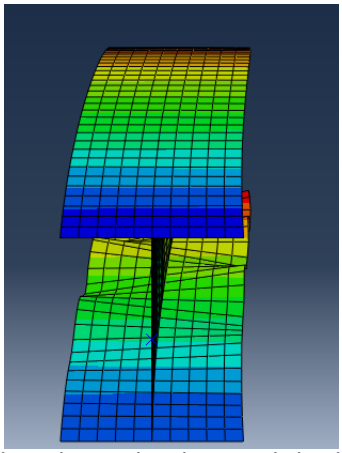

Figure 4.10: Deformed shape of the column when it can only buckle around the y-axis and in-plane deformations are allowed for Pcr,global,z= Pcr,global,y= Pcr,local.

From the curves “global mode (minor axis) with imperfections”, “global mode (major axis) with imperfections” and “local mode” represented in Figure 4.8, the local and global buckling modes exhibited stable load paths. However, the results from the curves “interaction between local and global,z modes” and “interaction between local and global,y modes” obtained by a model able to have in-plane deformations and global buckling over a defined axis, showed that the load path becomes unstable due to the interaction between local and global buckling modes.

Once the interaction between one global mode and the local mode was studied, interaction between local and global modes (with the two buckling axis) was analyzed. The results represent by the curve “interaction between modes” given by Figure 4.8 shows that the instability is reached more rapidly than considering only interaction between one global mode and the local mode. This means that there is some interaction between the global modes.

The deformed shape of the column when interaction between local and global buckling modes is allowed, is given by Figure 4.11

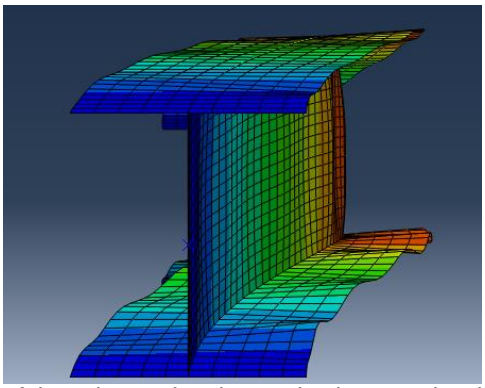

Figure 4.11: Deformed shape of the column when interaction between local and global buckling modes is allowed for Pcr,global,z= Pcr,global,y= Pcr,local.

From the results given by Figure 4.8 and presented until now, two problems are present: the interaction between global modes and the interaction of local mode with the global ones.

First, the results corresponding to “interaction between modes” and “interaction between global modes” from Figure 4.8 have only one difference: the possibility of in-plane deformations. By considering the results, it is possible to verify that local buckling has an impact on the interaction between global modes, by reducing the column’s stiffness (by the reduction of the geometric stiffness of the column).

Second by analyzing Figure 4.8 where the relation between the applied load and the maximum transverse displacement of the column is presented, the results given by the curve “interaction between global modes” may give the idea that there is no interaction between global buckling modes when observing the curve “global mode (minor axis) with imperfections”. Notice that no in-plane deformations are allowed for both curves.

Though both curves have the same load path as observed in Figure 4.8, it is important to remember that the displacements shown are the maximum transverse displacement but it doesn’t imply that there’s no interaction between global modes.

To have a better perception if there is any interaction between global modes, Figure 4.12 presents the relation between the applied load and the axial shortening of several possible models. The column used to produce the results displayed in Figure 4.12 was the same as the one defined in Table 4.6.

The interaction between global modes is clear by observing Figure 7.2 in annex B and by analyzing the curve “interaction between global modes” in Figure 4.12.

The interaction happens due to the following equation:

$$\sigma_N = \frac{P}{A} + \frac{P * v}{W_z} + \frac{P * w}{W_y} \tag{4.1}$$

Being P the axial force, v and w the displacement accounting already with the initial geometric imperfection in the y-direction and z-direction respectively and finally W_z and W_y are the section modulus.

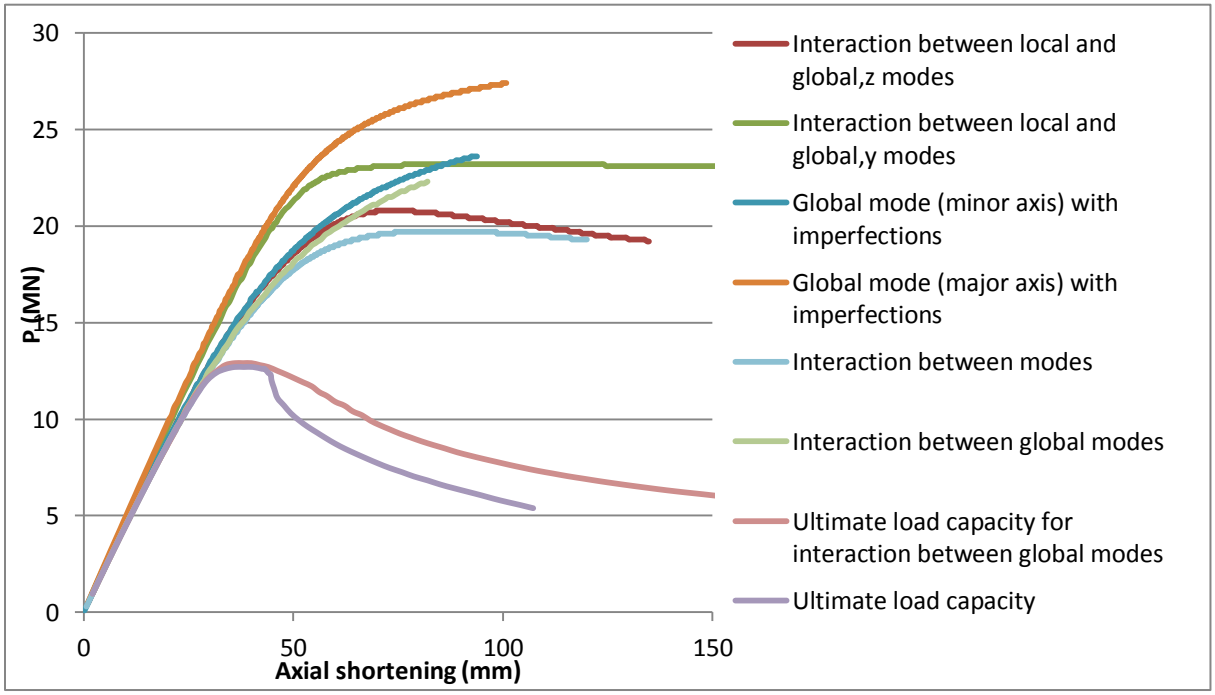

Figure 4.12: Load-axial shortening relation for Pcr,global,z= Pcr,global,y= Pcr,local .

When the imperfections are introduced, the column besides uniform compression, will have bending in both directions. Along with the axial shortening due to the uniform compression, an extra axial shortening should be added considering the fact that bending on both global axis will increase the deformation.

This fact can be observed by analyzing Figure 4.12. Curve “global mode (major axis) with imperfections” and “global mode (minor axis) with imperfections” only have axial shortening due to axial compression and bending around its own axis. When the column is allowed to deform globally, it will be allowed to bend around both axis and that is why the axial shortening will increase for the

same load. Therefore, it can be concluded that interaction between global buckling modes reduces the column's stiffness though the column remains stable.

Another question arose concerning interaction between global modes because Case I ($P_{cr,global,z}$= $P_{cr,global,y}$= $P_{cr,local}$) had similar global buckling loads. Therefore a different column was modeled in order to have different global buckling loads and if the global buckling loads are very different, there is no interaction or it is very small. All results are shown in Annex E.

Now that all the interaction between modes were explained for a column with similar buckling loads, it is necessary to evaluate the ultimate load from the FE model and compare it to the design value of the buckling resistance defined in the EC3 and given by Table 4.10:

Table 4.10: Design buckling resistance accordingly to the Eurocode 3.

Design buckling resistance by the Eurocode 3	
$N_{b,Rd}$ (MN)	12.96

The calculations regarding the EC3 guidance for the design load are shown in annex B.

As defined in the EC3, the ultimate load capacity of the FE models corresponds to the maximum load of the load path for "structures susceptible to buckling" (EN 1993-1-5:2006). The ultimate load capacity for a column with interaction between local and global buckling modes is given by Table 4.11. Concerning a column with interaction between only global buckling modes, the ultimate load capacity is given by Table 4.12.

Notice that the ultimate load capacity of the columns were evaluated based on the material being elastic perfectly plastic.

Table 4.11: Comparison between the ultimate load capacity of a column with interaction between local and global buckling modes for Pcr,global,z= Pcr,global,y= Pcr,local.

Ultimate load capacity (MN)	12.800
EC design buckling resistance (MN)	12.964
Difference (%)	1.265

Table 4.12: Comparison between the ultimate load capacity of a column with interaction between global buckling modes for Pcr,global,z= Pcr,global,y= Pcr,local.

Ultimate load capacity without in-plane deformations (MN)	12.900
EC design buckling resistance (MN)	12.964
Difference (%)	0.494

Table 4.11 and Table 4.12 show that the impact of having in-plane deformations due to local buckling in the ultimate load capacity of the FE model is quite reduced. Both tables also verify that the EC3 gives a reasonable approximation to the evaluation of the ultimate load capacity for the present example even when interaction between local and global buckling modes is present.

Case II ($P_{cr,global,z}= P_{cr,global,y}< P_{cr,local}$)

Case II ($P_{cr,global,z}= P_{cr,global,y}< P_{cr,local}$) is an example of a column which has both global buckling loads smaller than the local buckling load. Being the global buckling loads lower than the local buckling load, it is expected not to have a significant interaction between local and global buckling loads.

To perform that evaluation, the length of the column was increased considering the same cross-section properties (Table 4.5). Its length and buckling loads are given in Table 4.13.

Table 4.13: Column's length and buckling loads.

L (m)	34
$\overline{\lambda_z}$	0.954
$\overline{\lambda_y}$	0.941
$P_{cr,local}$ (MN)	31.322
$P_{cr,global,z}$ (MN)	21.826
$P_{cr,global,y}$ (MN)	22.960

The amplitudes adopted according to the EC3 are given in Table 4.14:

Table 4.14: Amplitudes for the column when Pcr,global,z= Pcr,global,y< Pcr,local.

Amplitudes	
Global buckling shape,z (L/200) (m)	0.1700
Global buckling shape,y (0.7*L/250) (m)	0.0952
Local buckling shape min (h/200; L/200) (m)	0.0033

The same analyzes as when the buckling loads were similar (Case I ($P_{cr,global,z}$= $P_{cr,global,y}$= $P_{cr,local}$)) were also performed in this section. The results are given in Figure 4.13.

Notice that the displacement displayed in Figure 4.13 is only the maximum transverse displacement of the column. It can be in the y-axis direction or the z-axis direction (Figure 3.5). For example the curve “interaction between local and global,y modes” has the z-axis displacement plotted in opposition to the curve “interaction between local and global,z modes” that has the y-axis displacement plotted because the maximum transverse displacements occur in the z-axis and y-axis respectively.

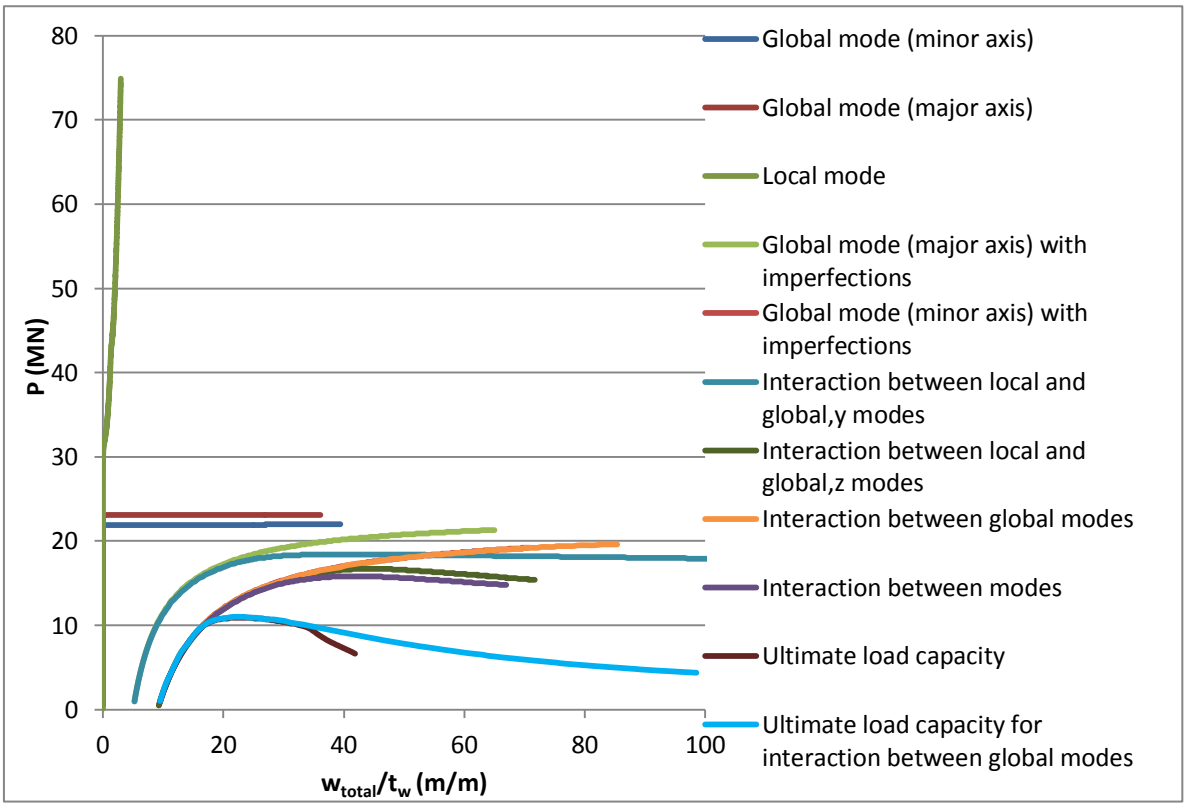

Figure 4.13: Load-displacement for Pcr,global,z= Pcr,global,y< Pcr,local.

The deformed shape of the column for the curve “interaction between local and global,z modes” and for the curve “interaction between local and global,y modes” are given in annex C (Figure 7.9 and Figure 7.10).

It can be observed from curve “interaction between local and global,z modes” and “interaction between local and global,y modes” represented in Figure 4.13 that even with the local buckling load significantly higher than the global buckling loads, the introduction of geometric imperfections regarding local buckling and the fact that in-plane deformations are allowed introduces instability on the column. Although, for the buckling modes in separate, the column’s behavior is stable.

Case II ($P_{cr,global,z}$= $P_{cr,global,y}$< $P_{cr,local}$) has a difference between the local and global buckling loads, being the global buckling modes the governing modes. Therefore, due to that difference, it was expected that the interaction between local and global modes would be less important when compared to Case I ($P_{cr,global,z}$= $P_{cr,global,y}$= $P_{cr,local}$).

By analyzing the curve “interaction between modes” and “interaction between global modes” from Case I ($Pcr_{,global,z}$= $Pcr_{,global,y}$= $Pcr_{,local}$) and Case II ($Pcr_{,global,z}$= $Pcr_{,global,y}$< $Pcr_{,local}$) given by Figure 4.8 and Figure 4.13 respectively, it was verified that indeed the interaction between local and global buckling mores is slightly amplified when the buckling loads are similar. This was concluded when comparing the curve “interaction between modes” and “interaction between global modes” given by Figure 4.8 for Case I ($Pcr_{,global,z}$= $Pcr_{,global,y}$= $Pcr_{,local}$) where the column becomes unstable sooner than in the Case II ($Pcr_{,global,z}$= $Pcr_{,global,y}$< $Pcr_{,local}$).

As observed in Case I ($P_{cr,global,z}$= $P_{cr,global,y}$= $P_{cr,local}$) and in the curve “interaction between modes” given by Figure 4.13, when interaction between both global modes and the local mode is allowed, the column becomes unstable sooner than if the column was only able to have one global buckling axis and in-plane deformations. This indicates that interaction between global modes is occurring.

To have a different perspective on how the buckling modes interact, the relation between the applied load and axial shortening of the column is represented in Figure 4.14.

It can be observed that interaction between global modes occurs. Also by comparing the results of curve “interaction between local and global,y modes” and “interaction between local and global,z modes” given by Figure 4.14, it is verified that the in-plane deformation from local buckling has an impact on the load path when a single global mode and the local one are interacting.

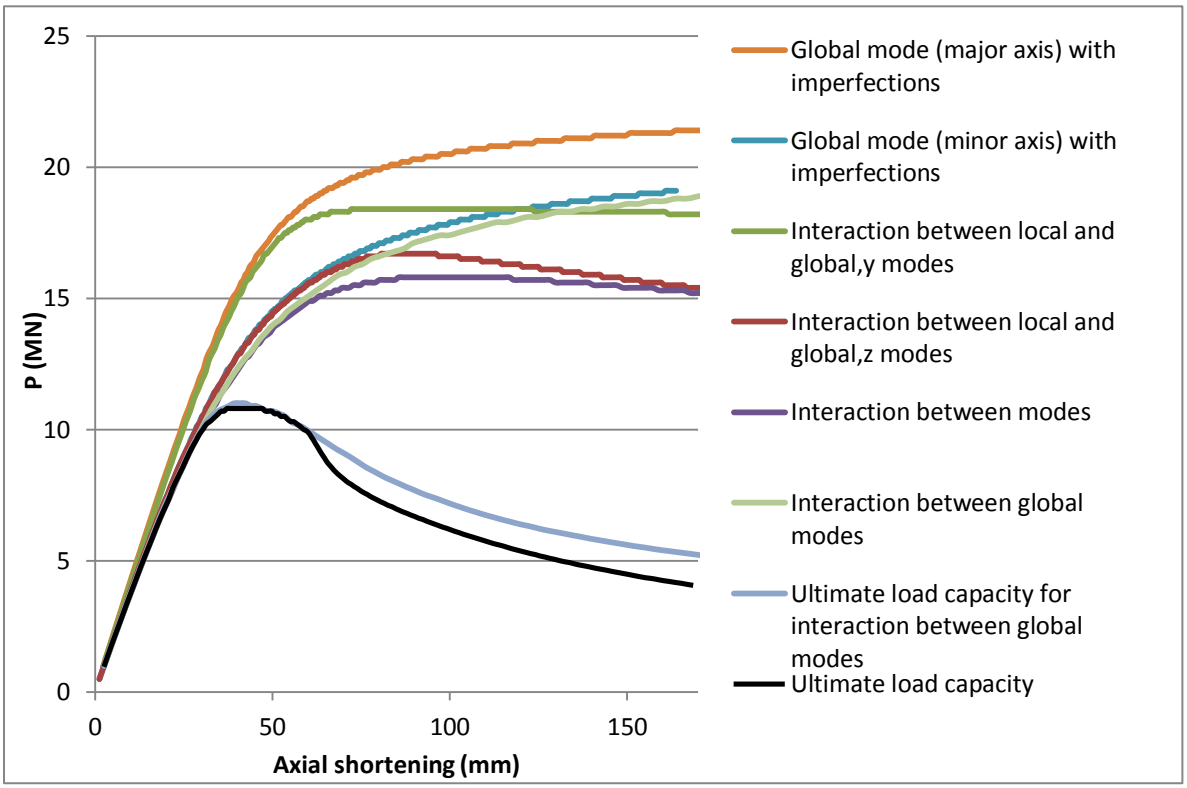

Figure 4.14: Load-axial shortening relation for Pcr,global,z= Pcr,global,y< Pcr,local .

The resistant load obtained from the EC3 compared to the ultimate load obtained from the FE model allowed to have interaction between local and global buckling modes and compared to the FE model prevented to have in-plane deformations is given by Table 4.15 and Table 4.16.

Table 4.15: Comparison between the ultimate load capacity of a column with interaction between local and global buckling modes for Pcr,global,z= Pcr,global,y< Pcr,local.

Ultimate load capacity (MN)	10.900
EC design buckling resistance (MN)	11.370
Difference (%)	4.130

Table 4.16: Comparison between the ultimate load capacity of a column with interaction between global buckling modes for Pcr,global,z= Pcr,global,y< Pcr,local.

Ultimate load capacity without in-plane deformations (MN)	11.000
EC design buckling resistance (MN)	11.370
Difference (%)	3.251

From the results presented in Table 4.15 and Table 4.16, it's possible to verify that the difference between the ultimate load from the FE models and the resistant load obtained from the EC3 is higher than in Case I ($Pcr_{,global,z}$= $Pcr_{,global,y}$= $Pcr_{,local}$) where critical loads were similar.

A possible explanation may be related to EC3's guidance to evaluate the buckling resistance of the column. The EC3 does not take into consideration the two global geometric imperfections that were introduced in the FE model in the two global buckling axes. Instead, the EC3 only evaluates the buckling resistance based on a single global geometric imperfection. In fact, having two global geometric imperfection for the two buckling axis, it can increase the impact of the interaction between global buckling modes on the reduction of the column's stiffness and consequently increasing the column's instability.

For a non-linear analysis with an elastic perfectly plastic material, the EC3 defines the ultimate load capacity of the column as being the maximum load for the load path. Being both global geometric imperfections present in the column and by having a reduction on the column's stiffness, the maximum load from the non-linear analysis may be smaller than the buckling resistance obtained from the EC3.

Being this explanation applied for all the EC3 calculations (in Case I ($P_{cr,global,z}$= $P_{cr,global,y}$= $P_{cr,local}$), Case II ($P_{cr,global,z}$= $P_{cr,global,y}$< $P_{cr,local}$) and Case III ($P_{cr,global,z}$= $P_{cr,global,y}$> $P_{cr,local}$)) for obtaining the buckling resistance, the effect of the global geometric imperfections will be more relevant for higher levels of slenderness, because global buckling will govern the buckling phenomenon for this particular study. In Case II ($P_{cr,global,z}$= $P_{cr,global,y}$< $P_{cr,local}$), the difference between the ultimate load and the buckling resistance is higher due to the interaction between buckling modes. For Case I ($P_{cr,global,z}$= $P_{cr,global,y}$= $P_{cr,local}$) though the buckling loads are similar, interaction between global modes is verified. However, the difference between the ultimate load capacity of the column from the interaction between global modes and the buckling resistance obtained from the EC3 is quite reduced (Table 4.12). This small difference may be explained by the conservative use of the effective width and the yielding criterion by the EC3 (explanation will be more developed in Case III ($P_{cr,global,z}$= $P_{cr,global,y}$> $P_{cr,local}$)) tough for higher levels of the column's slenderness (being the interaction between global modes more significant), the EC3 is not able to consider effectively the interaction between global buckling modes.

Case III ($P_{cr,global,z}= P_{cr,global,y}> P_{cr,local}$)

Case III ($P_{cr,global,z}= P_{cr,global,y}> P_{cr,local}$) is an example where the global buckling loads are higher than the local buckling load. To this end, the column's length was decreased. The length and buckling loads are given in Table 4.17.

Table 4.17: Column's length and buckling loads.

L (m)	22
$\overline{\lambda_z}$	0.618
$\overline{\lambda_y}$	0.609
$P_{cr,local}$ (MN)	31.248
$P_{cr,global,z}$ (MN)	51.782
$P_{cr,global,y}$ (MN)	53.683

The geometric imperfections of the column were defined by the EC3, being the corresponding amplitudes of the buckling shape given by Table 4.18.

Table 4.18: Amplitudes for the column when Pcr,global,z= Pcr,global,y> Pcr,local.

Amplitudes	
Global buckling shape,z (L/200) (m)	0.1100
Global buckling shape,y (0.7*L/250) (m)	0.0616
Local buckling shape min (h/200; L/200) (m)	0.0033

As presented in Case I ($P_{cr,global,z}= P_{cr,global,y}= P_{cr,local}$) and Case II ($P_{cr,global,z}= P_{cr,global,y}< P_{cr,local}$), the results in terms of the applied load and the maximum transverse displacement for several FE models are given by Figure 4.15.

For this example, the local buckling mode is the governing phenomenon. Therefore the interaction of global modes is much smaller when compared to the impact of local buckling. The results represented by the curves "interaction between modes" and "interaction between global modes" given by Figure 4.15 allows to verify that the local buckling mode has a more significant impact on the load path of the column than the global modes.

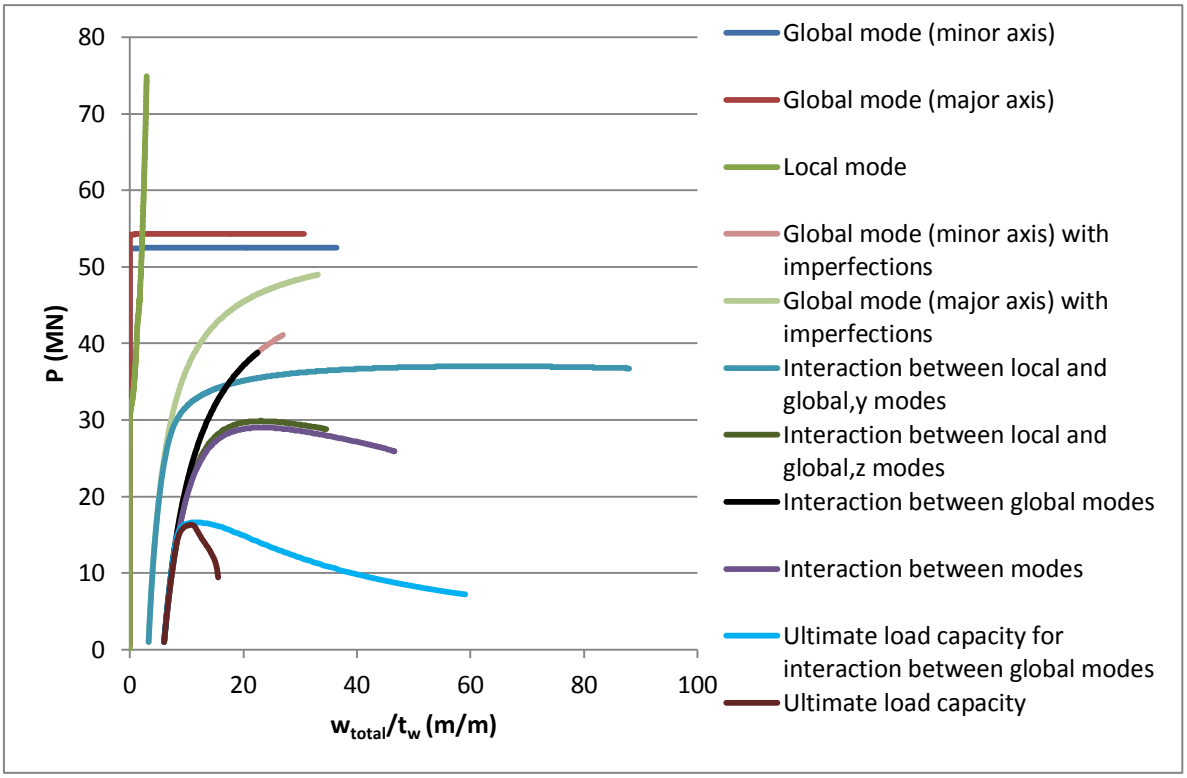

Figure 4.15: Load-displacement for Pcr,global,z= Pcr,global,y> Pcr,local.

Returning to the previous examples already analyzed (Case I ($Pcr_{,global,z}$= $Pcr_{,global,y}$= $Pcr_{,local}$) and Case II ($Pcr_{,global,z}$= $Pcr_{,global,y}$< $Pcr_{,local}$)), for Case I ($Pcr_{,global,z}$= $Pcr_{,global,y}$= $Pcr_{,local}$), the column's instability was reached for a load much closer to the local buckling load than for Case II ($Pcr_{,global,z}$= $Pcr_{,global,y}$< $Pcr_{,local}$). Due to this fact, the local buckling mode when interacting with the global modes has a more significant impact on the column's stability, being the instability reached sooner when the local buckling load is similar to the governing global mode.

In this present case, Case III ($P_{cr,global,z}$= $P_{cr,global,y}$> $P_{cr,local}$), as presented in Figure 4.15 by the curve "interaction between modes", the column becomes unstable for a load closer to the local buckling load in comparison to Case I ($Pcr_{,global,z}$= $Pcr_{,global,y}$= $Pcr_{,local}$) and Case II ($Pcr_{,global,z}$= $Pcr_{,global,y}$< $Pcr_{,local}$). Therefore, the amplification of the interaction between local and global modes and consequently the column's instability has a more significant impact for when local buckling modes are governing.

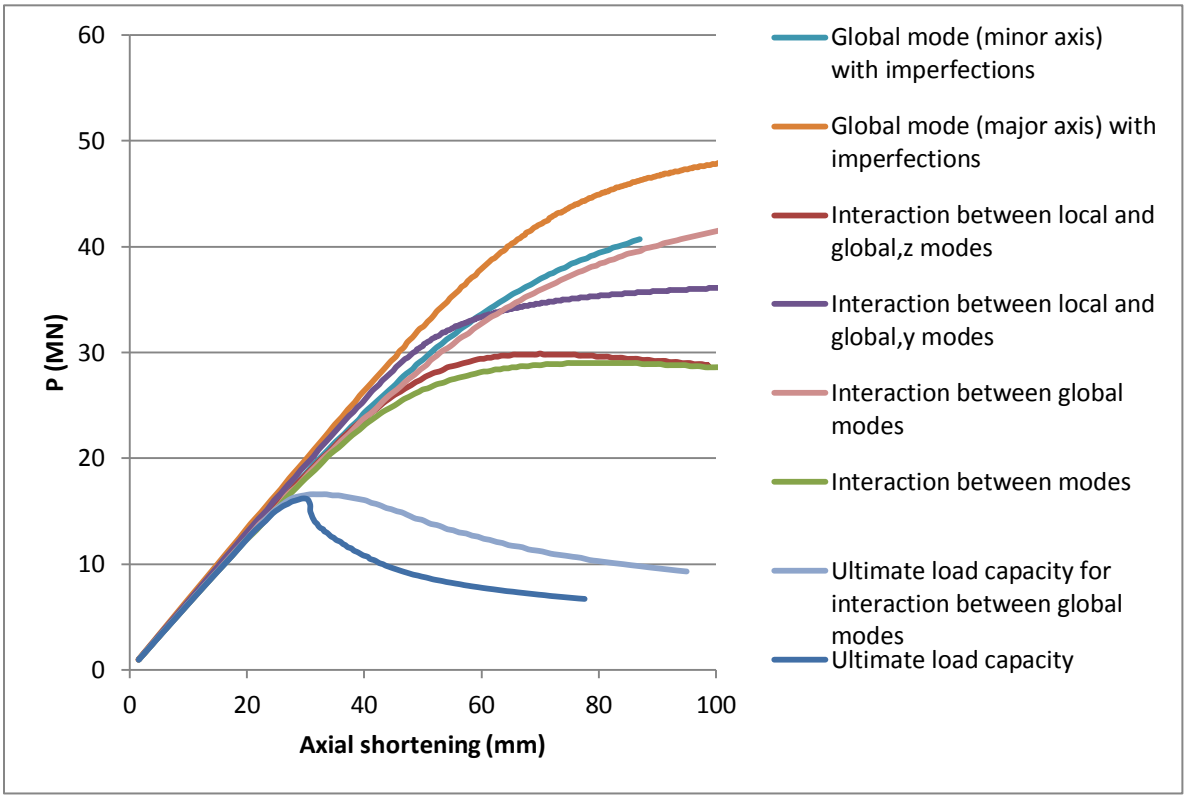

Figure 4.16: Load-axial shortening relation for Pcr,global,z= Pcr,global,y> Pcr,local .

The ultimate load capacity from the interaction between local and global modes obtained from the FE model and the design buckling resistance evaluated by the EC3 are given by Table 4.19. Also a comparison of the ultimate load capacity obtained from the FE model for which the column was not allowed to have in-plane deformations and the resistance given by the EC3 is given in Table 4.20.

Table 4.19: Comparison between the ultimate load capacity of a column when it's free to have in-plane deformations, considering the geometric imperfection and the Eurocode's value for Pcr,global,z= Pcr,global,y> Pcr,local.

Ultimate load capacity (MN)	16.300
EC design buckling resistance (MN)	15.545
Difference (%)	-4.858

Table 4.20: Comparison between the ultimate load capacity of a column without in-plane deformation, considering the geometric imperfection and the Eurocode's value for Pcr,global,z= Pcr,global,y> Pcr,local.

Ultimate load capacity without in-plane deformations (MN)	16.6
EC design buckling resistance (MN)	15.545
Difference (%)	-6.788

In this case the difference between the EC3 load and the ultimate load capacity is the lowest one compared to Case I ($Pcr_{,global,z}$= $Pcr_{,global,y}$= $Pcr_{,local}$) and Case II ($Pcr_{,global,z}$= $Pcr_{,global,y}$< $Pcr_{,local}$), being even the ultimate load capacity from the FE model higher than the resistance load from the EC3.

The reason of the ultimate load capacity being higher than the buckling resistance evaluated by the EC3 may be due to the fact that the EC3 evaluates the resistance based on the yielding of the column and based on the effective width concept. In the FE model, despite the yielding of the column, the column will have a capacity of supporting more load and the ultimate load capacity for the FE model is evaluated based on the maximum load resultant from the non-linear analysis. On the other hand, the EC3 by the use of the effective width concept reduces the cross-section of the column. Therefore the buckling resistance will be reduced. Being the column able to support more load after the starting point of yielding and considering that plates have a post-buckling increase of strength, the ultimate load capacity of the column obtained from a non-linear analysis performed by the FE model may be higher than the buckling resistance from the EC3.

4.3.2 Column: Parametric study

Based on Case I ($P_{cr,global,z}$= $P_{cr,global,y}$= $P_{cr,local}$), Case II ($P_{cr,global,z}$= $P_{cr,global,y}$< $P_{cr,local}$) and Case III ($P_{cr,global,z}$= $P_{cr,global,y}$> $P_{cr,local}$) it was possible to evaluate the interaction between local and global buckling modes and compare the ultimate load capacity obtained from the three cases to the buckling resistance given by the EC3.

From the three cases, it was verified that interaction between local and buckling modes caused instability of the column. The results from Case I ($P_{cr,global,z}$= $P_{cr,global,y}$= $P_{cr,local}$), Case II ($P_{cr,global,z}$= $P_{cr,global,y}$< $P_{cr,local}$) and Case III ($P_{cr,global,z}$= $P_{cr,global,y}$> $P_{cr,local}$) demonstrate that when the local buckling load was similar or even lower than the global buckling loads, the column's instability was reached comparatively sooner than for the case when the local load was higher than the global ones.

The comparison between the ultimate load capacities obtained from the non-linear analysis for the three cases and the resistance obtained from the EC3 showed that with the increasing of the column's length, the evaluation of the buckling resistance obtained from the EC3 resulted in higher values of the resistance compared to the ultimate load capacity from the FE models.

The three cases previously analyzed were relevant to verify the interaction between buckling modes. However, only three cases weren't representative of the interaction between buckling modes and the comparison to the EC3 buckling resistance. Therefore, more information was

needed. By conducting a parametric study for the same cross-section defined for the three cases (Case I ($P_{cr,global,z}$= $P_{cr,global,y}$= $P_{cr,local}$), Case II ($P_{cr,global,z}$= $P_{cr,global,y}$< $P_{cr,local}$) and Case III ($P_{cr,global,z}$= $P_{cr,global,y}$> $P_{cr,local}$)) and presented in Table 4.5, it was possible to evaluate the ultimate load capacity obtained from the FE models and compare it to the EC3 for a wider range of lengths.

The results of the parametric study are presented in Figure 4.17. The Eurocode's buckling resistances were also obtained and the calculations are presented in annex F.

In Figure 4.17 different types of results are represented by several curves. Curve "EC buckling resistance" represents the EC3's buckling resistances obtained based on the guidance from the EC3.

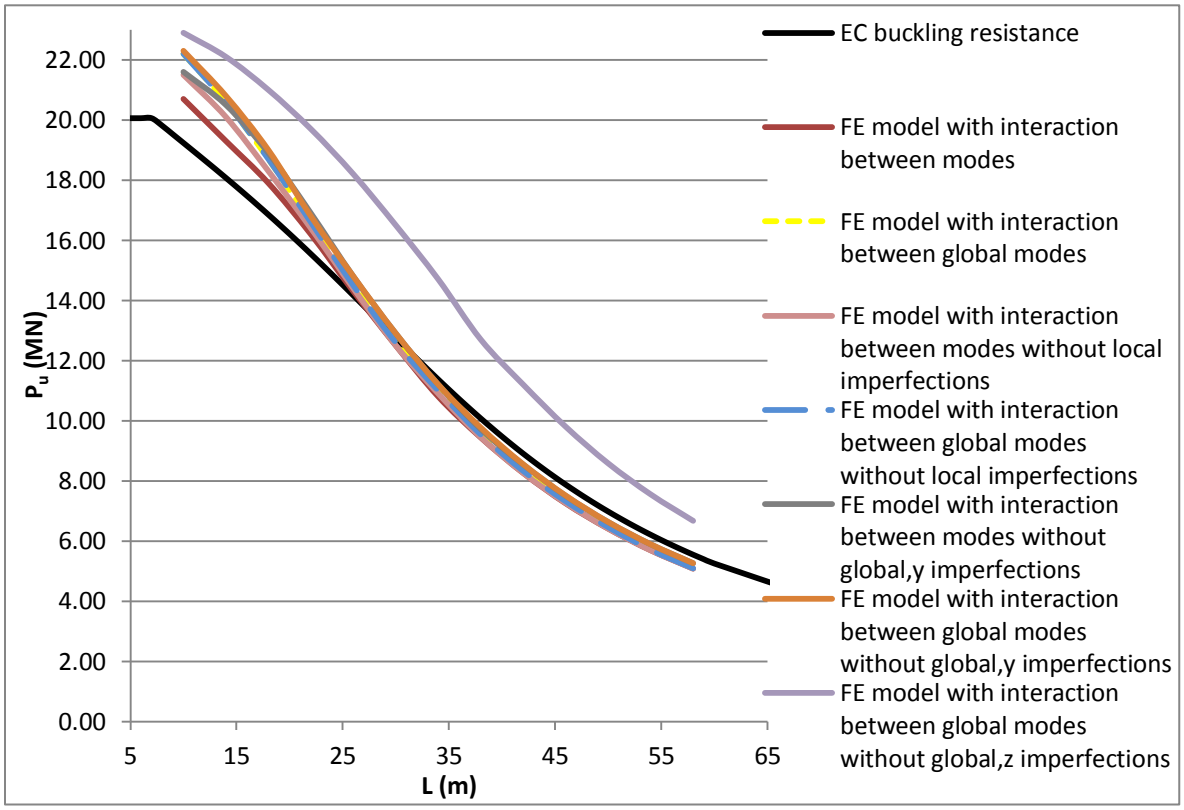

Figure 4.17: Parametric study for the column and comparison between the Eurocode.

It is clear from Figure 4.17 and Table 4.21 that the EC3, for this particular cross-section, can predict the buckling resistance for the less slender columns when compared to the curve "FE model with interaction between modes". This curve represents the results regarding the ultimate load capacity for a FE model able of having interaction between local and global buckling modes.

Table 4.21: Difference between the FE model and the EC.

L (m)	Difference between the FE model and the EC (%)
10	-7.60
14	-6.78
18	-6.22
22	-4.21
26	-0.95
30	1.98
34	5.01
38	6.30
42	7.24
46	7.92
50	8.14
54	8.33
58	8.37

Based on the experimental and numerical investigation developed by Becque & Rasmussen (Becque & Rasmussen, 2009), it is possible to perform a qualitative comparison regarding the results presented in Figure 4.17.

The investigation developed by Becque & Rasmussen (Becque & Rasmussen, 2009), studied the interaction between local and global buckling in a stainless steel (with a non-linear behavior, anisotropy and increased corner properties due to cold working) column. A FE analysis was performed for back-to-back channels in compression, in order to predict the ultimate load capacity of a simply supported column. Several parametric studies for an extensive range of column's slenderness were conducted by Becque & Rasmussen (Becque & Rasmussen, 2009) considering different types of stainless steels. The ultimate load capacity results were compared to several design codes including the European code. Becque & Rasmussen concluded that although the EC3 achieve good predictions of the ultimate load capacity for small values of slendernee, the EC3 failed to predict safely the interaction between modes for high values of the column's slenderness.

The work performerd by Becque & Rasmussen (Becque & Rasmussen, 2009) though it has different type of material and cross-section, the results and conclusions from (Becque & Rasmussen, 2009) can be qualitatively compared to the results obtained from the FE analysis presented by Figure 4.17.

By comparing the results from the curves “EC buckling resistance” and “FE model with interaction between modes”, from Figure 4.17 and Table 4.21, the EC3 is conservative on the evaluation of the buckling resistance for small lengths of the column.

A possible reason for the conservative values of the buckling resistance obtained from the EC3 is the fact that the EC3 evaluates resistance based on the yielding of the column and based on the effective width although the column can resist to a higher load until it becomes unstable, whereas the FE model obtains the ultimate load capacity from the applied load for which the column becomes unstable, as defined in the EC3 for a FE analysis. For higher values of the slenderness ratio, the interaction between global buckling modes is more relevant therefore, even the use of the yielding criterion and the effective width, may be not sufficient to predict the buckling resistance.

Table 4.22 presents the ultimate load capacity and the load for which the first finite element start to yield, corresponding to the results obtained from the curve “FE model with interaction between modes”. The difference between the loads in Table 4.22 indicates that the column is able to resist to a much higher load than the yielding load, mainly for lower values of the column’s slenderness.

Table 4.22: Comparison between the ultimate load from the FE model and the load for which yielding starts.

L (m)	P_u of the FE model able to have interaction between modes (MN)	P (MN) for the 1º yielding element of the FE model able to have interaction between modes
10	20.70	16.00
14	19.30	14.80
18	17.90	13.50
22	16.20	12.40
26	14.30	11.00
30	12.50	9.83
34	10.80	8.76
38	9.44	7.82
42	8.26	6.99
46	7.25	6.26
50	6.41	5.63
54	5.69	5.07
58	5.08	4.58

Concerning higher values for the column’s length, the EC3 appears not to predict conservatively the buckling resistance for the column for this particular cross-section as defined in Table 4.5, being a possible explanation, the impact of the interaction between global modes.

Being the curve “FE model interaction between global modes” and the curve “FE model with interaction between global modes without global,y imperfections” modeled without in-plane deformations, its results can evaluate the impact of interaction between global modes.

By analyzing the results represented by the curve “FE model interaction between global modes” and the curve “FE model with interaction between global modes without global,y imperfections”, it is possible to verify that for the model which has only global buckling over the minor axis (curve “FE model with interaction between global modes without global,y imperfections”), the results of the buckling resistance regarding the EC3 for higher lengths of the column are similar to the results obtained from the FE model. Therefore, it is possible that the EC3 does not consider the interaction between global buckling modes because the guidance given by the EC3 to evaluate the buckling resistance only considers one buckling plane and the corresponding geometric imperfection for that plane, whereas the FE analysis was performed with global geometric imperfections for the two global buckling planes.

Concerning the impact of local imperfections, its impact will be different depending on the column’s slenderness although it was verified from the previous examples (Case I ($P_{cr,global,z}= P_{cr,global,y}= P_{cr,local}$) to Case III ($P_{cr,global,z}= P_{cr,global,y}> P_{cr,local}$)) that the interaction between local and global modes results in the instability of the column. The impact can be observed based on the results from the curves “FE model with interaction between modes” and “FE model with interaction between modes without local imperfections”.

The impact of local geometric imperfection will result in a smaller ultimate load capacity from the curve “FE model with interaction between modes” in comparison to the curve “FE model with interaction between modes without local imperfections”.

For small values of the column’s slenderness, being the local buckling mode the governing mode, local geometric imperfections will have a significant impact on the ultimate load capacity thus the ultimate load capacity will be reduced compared to the load from the curve “interaction between global modes”. For higher values of the column’s slenderness, the impact of local geometric imperfections will decrease because the column’s buckling will be governed by the global mode.

For a particular length (42 meters), the results from Figure 4.17 were analyzed, being presented further below in detail.

By evaluating the normal stresses due to the axial force and the normal stresses due to bending on both directions based on equation (4.2), it was possible to compare several FE models: the FE model with interaction between local and global buckling modes without local imperfections, the FE model with interaction between global modes without local imperfections and the normal stresses

were also obtained from the FE model with interaction between global buckling modes without local imperfections and global imperfections on the major buckling axis.

From the FE analysis, the transverse displacements are known as well as the applied load. Therefore it was possible to obtain the maximum normal stress at the cross-section in the middle of the column by applying equation (4.2).

$$\sigma_N = \frac{P}{A} + \frac{P * v}{W_z} + \frac{P * w}{W_y} \tag{4.2}$$

Being P the axial force, v and w the displacement with the initial geometric imperfection in the y-direction and z-direction respectively and finally W_z and W_y are the section modulus (defined in the annex F).

For the FE model with interaction between local and global buckling modes without local imperfections, the initial geometric imperfections and the transverse displacements of the middle point of the column are given by Table 4.23.

Notice that w_0 represents the initial geometric imperfection at the z-direction (Figure 3.3) and w the displacement at the z-direction. The initial geometric imperfection at the y-direction and the corresponding displacement are given by v_0 and v.

Table 4.23: Initial geometric imperfections and transverse displacements of the middle of the column for the FE model with interaction between local and global buckling modes without local imperfections.

w_0 (m)	**v_0 (m)**
0.1176	0.1050
w(m)	**v (m)**
0.1096	0.2106

Table 4.24 presents the normal stresses for the FE model with interaction between local and global buckling modes without local imperfections. Notice that the total normal stress presented in Table 4.24 and in the other tables below are almost equal to the yielding stress, being the difference probably due to the level of accuracy of the FE analysis.

Table 4.24: Normal stresses due to the axial force and bending for a FE model with interaction between local and global buckling modes without local imperfections.

P (MN)	7.17
σ_N (MPa)	104.63
σ_{My} (MPa)	208.52
σ_{Mz} (MPa)	61.24
σ_{total}(MPa)	374.39

Concerning the FE model with interaction between global modes without local imperfections, Table 4.25 presents the geometric imperfections of the column. The normal stresses due to axial force and bending are given by Table 4.26.

Comparing the results from Table 4.24 and Table 4.26, it is possible to verify that the FE with interaction between modes presents a lower yielding load (though the difference is almost insignificant) in comparison to the FE model with interaction between global modes. Therefore, in-plane deformations associated with the local buckling mode is responsible for the reduction of the yielding load and consequently it also has an impact on the ultimate load capacity of the column.

Table 4.25: Displacement of the middle point of the column with interaction between global modes without local imperfections.

v (m)	w (m)
0.2107	0.1083

Table 4.26: Normal stresses due to the axial force for a FE model with interaction between global buckling modes without local imperfections.

P (MN)	7.20
σ_N (MPa)	105.13
σ_{My} (MPa)	209.56
σ_{Mz} (MPa)	61.18
σ_{total}(MPa)	375.86

Regarding the impact of having two global geometric imperfections present in the column, the normal stresses of the FE model with interaction between global buckling modes without local imperfections and global imperfections on the major buckling axis was compared to the normal

stresses of the FE model with interaction between global modes without local imperfections presented in Table 4.26.

The initial geometric imperfections and the displacements of the FE model without local imperfections and global imperfection on the major buckling plane is given by Table 4.27.

Table 4.27: Initial geometric imperfections and transverse displacements of the middle of the column without local imperfections and global,y imperfections.

w_0 (m)	v_0 (m)
0	0.1050
w(m)	**v (m)**
0	0.2643

The normal stresses of the FE model with interaction between global buckling modes are given by Table 4.28.

Table 4.28: Normal stresses due to the axial force for a FE model with interaction between global buckling modes without local imperfections and globa,y imperfections.

P (MN)	8.03
σ_N **(MPa)**	117.28
σ_{My} **(MPa)**	263.56
σ_{Mz} **(MPa)**	0.00
σ_{total}**(MPa)**	380.84

Comparing Table 4.26 and Table 4.28, it is verified that the yielding load is lower for the FE model with interaction between global modes without local imperfections when compared to the FE model with interaction between global buckling modes without local imperfections and global imperfections on the major buckling axis. Consequently, the ultimate load capacity of the FE model with interaction between global modes with global imperfections on both global buckling planes will be lower compared to the FE model without the global imperfection on the major buckling plane, indicating that there will be interaction between global modes when global geometric imperfections are introduced in both global buckling planes in the FE model.

5 Conclusions

The objective of this thesis was to study the interaction between local and global buckling modes of thin-walled steel structures. Therefore a small summary of the theory behind the buckling modes was necessary. The first chapters explained all the theory behind the buckling phenomenon.

The thesis began by study the thin plates' theory. The critical buckling load for a simply supported plate uniaxial compressed and for a simply supported plate with one longitudinal edge free was derived. These two examples functioned as boundaries for the I shape cross-section that was studied along this entire thesis. The flanges could be so small compared to the web that in the limit the web would function as a simply supported plate. On the other hand, the web could be so small that in the limit, it would work as simple support for the flange.

With this in mind, the critical buckling load for an I-section was derived. The limits set by the two extreme examples (simply supported plate and simply supported plate with one longitudinal edge free) were almost correct except for a certain range of the flanges' width. For that range, it is possible that the flanges may work as stiffeners for the web.

After obtaining the critical buckling loads for the I-section, the post-buckling of plates was studied based on von Kármán's theory. The effective width concept was also studied.

Being the subject of this thesis the interaction between local and global buckling modes, an overview of global buckling of columns was also necessary. Beam's theory was studied with special attention to the Euler's buckling load and its post-buckling behavior.

The EC3's guidance for the design buckling resistance of a compressed member and the guidance given in order to perform a nonlinear analysis by a finite element software was very important for this thesis. Therefore, a section regarding the Eurocode guidelines for the geometric imperfections, the cross-section classifications and how to calculate the design buckling load, was introduced in this thesis.

A matter of great importance was also the finite element modeling. The finite element models were implemented with the help of the Abaqus software. All the modeling was described: the functions used from the software; the mesh; the geometric and material properties; geometric imperfections; boundary and load conditions.

Since the finite element models were adopted to study stability of thin-walled structures, its validation was necessary. Therefore the validation of the finite element models of a simply

supported plate and a simply supported I-column was performed. The buckling loads of the two examples from the FE model were compared to the theoretical calculations as well as the post-buckling load for the simply supported plate. Due to the small differences between the numerical and the theoretical results, the models were validated and used to study the interaction between buckling modes.

In order to study the interaction between local and global buckling modes of a thin-walled steel open section column, an I-section column with similar buckling loads was defined, being the column required to satisfy several conditions: cross-section classified as class 4; accounting to the web should be the plate governing; and the local buckling shape should have the maximum transverse displacement at the middle of the column in order to increase the maximum displacement when the column was buckling globally.

So a very uncommon I-column with three different lengths was defined. These three different lengths were defined in order to achieve three very important situations: one for which all buckling loads were similar; one to have the global buckling loads lower than the local buckling load and the final one to have a local buckling load lower than the global ones.

By analyzing the results from the three cases (Case I ($Pcr_{,global,z}$= $Pcr_{,global,y}$= $Pcr_{,local}$), Case II ($Pcr_{,global,z}$= $Pcr_{,global,y}$< $Pcr_{,local}$) and Case III ($Pcr_{,global,z}$= $Pcr_{,global,y}$> $Pcr_{,local}$)) and afterwards the results from the parametric study, it was verified that there is interaction between local and global buckling modes. The interaction between modes results in a reduction of the column's stiffness leading to the column's instability although the column presents a stable behavior when local or global buckling modes are present.

The comparison between the ultimate loads from the FE analysis and the design buckling loads from the EC3 showed that for small levels of the slenderness ratio, the use of the effective width by the EC3 was conservative in terms of the evaluation of the buckling resistance, despite the differences of the methodologies used to obtain the ultimate load capacity from the FE analyses and the resistance from the EC3. The Eurocode uses the yielding criterion of the cross-section to obtain the buckling resistance and the guidance given by the same Eurocode to perform a finite element analysis with nonlinearity, uses the criterion of the maximum load before instability occurs to obtain the ultimate load.

For higher values of the slenderness ratio, the impact of the local buckling mode as well as the local geometric imperfections is lower than the one verified for lower values of the column's slenderness. Although it was verified that the ultimate load was lower than the EC3 buckling resistance but the differences were not substantial.

The reason for the EC3 buckling resistance being higher than the ultimate load obtained from the FE analysis is due to the interaction between global buckling modes and due to a possible impact of in-plane deformations.

The results of the ultimate load capacity from the FE analysis were obtained from a model which had two global geometric imperfections, one imperfection for each global buckling plane. On the other hand, the EC3 does not take into consideration the two global geometric imperfections for the evaluation of the design buckling resistance. Therefore, it is possible that by introducing the two global imperfections, the ultimate load capacity will be lower than the resistance obtained from the EC3.

The impact of having two global geometric imperfections on the FE model was verified by analyzing a FE model with no in-plane deformations therefore it was not influenced neither by the local buckling mode nor by the local geometric imperfections and by analyzing a FE model with no in-plane deformations and without the global geometric imperfection over the major buckling plane. The results showed that by not considering the global imperfection over the major buckling axis, the ultimate load capacity was similar to the EC3 buckling resistance.

The conclusion of the finite element analysis performed is that two types of interaction in the I-column were present: interaction between local and global modes and interaction between global modes.

Interaction between local and global modes is limited and its importance only increases to low values of the column's slenderness although the interaction introduces an unstable behavior on the column and the EC3 buckling resistance is conservative for small values of the slenderness ratio.

When global modes interact between each other, especially for higher values of the column's slenderness, the Eurocode may not predict conservatively the buckling resistance though the differences between the EC3 resistance and the results from the FE analysis were not significant.

Despite the conclusions presented above, it is important to continue the study of the interaction between buckling modes and the comparison of the results to the Eurocode buckling resistance. Therefore, several studies should be performed.

A further study of the interaction between local and global buckling modes through a theoretical formulation should be made. Experimental investigations should be performed to validate the numerical results. And finally different supports and load conditions should be also studied in order to verify if the conclusions deduced from this thesis can be extrapolated to other examples.

6. References

Abaqus 6.13 Documentation. (s.d.). Simulia.

Anbarasu, M., & Sukumar, S. (2014). Local/Distortional/Global Buckling Mode Interaction on thin Walled Lipped Channel Columns. *Latin American Journal of Solids and Structures*, 1363-1375.

Becque, J., & Rasmussen, K. J. (2009). Numerical Investigation of the Interaction of Local and Overall Buckling of Stainless Steel I-Columns. *JOURNAL OF STRUCTURAL ENGINEERING*, 1349-1356.

Bloom, F., & Coffin, D. (1944). *Handbook of Thin Plate Buckling and Postbuckling.* Boca Raton, Florida: CRC Press LLC.

Bulson, P., & Allen, H. (1980). *Backgrounf to Buckling.* London, New York: McGraw-Hill Book Co.

Chages, A. (1974). *Principles of Structural Stability Theory.* Englewood Cliffs: Prentice-Hall.

EN 1993-1-1:2005. (s.d.).

EN 1993-1-5:2006. (s.d.).

Ioannidis, G., & Kounadis , A. (1994). Lateral Post-Buckling Analysis of Monosymmetric 1-Beams under Uniform Bending. *J. Construct. Steel Research* .

Kiymaz, G. (2005). FE based mode interaction analysis of thin-walled steel box columns under axial compression. *Thin-walled structures*, 1051-1070.

Koiter, W. (1945). *Over de stabiliteit van het elastisch evenwicht.* Delft: Delft thesis; (English transl.) Nat. Aeronaut. Space Admin. Rep. TTF-10, 1967.

Macdonald, M., Heiyantuduwa, M., & Rhodes, J. (2008). Recent developments in the design of cold-formed steel members. *Thin-Walled Structures*, 1047– 1053.

Mohri, F., Eddinari, A., Damil, N., & Potier Ferry, M. (2008). A beam finite element for non-linear analyses of thin-walled elements. *Thin-Walled Structures*, Volume 46, Issues 7-9, Pages 981-990.

Pilkey, W., & Wunderlich, W. (1994). *Mechanics of Structures - Variational and Computational Methods.* Boca Raton: CRC Press.

Reis, A., & Camotim, D. (2001). *Estabilidade Estrutural.* Lisbon: McGraw-Hill de Portugal.

Schafer, B. W. (March 2002). Local, Distortional, and Euler Buckling of Thin-Walled. *JOURNAL OF STRUCTURAL ENGINEERING*, 289-299.

Timoshenko, S., & Gere, J. (1961). *Theory of Elastic Stability.* New York: McGraw-Hill.

Timoshenko, S., & Goodier, J. (1970). *Theory of Elasticity.* Singapore: McGraw-Hill, third edition.

Timoshenko, S., & Woinowsky-Krieger, S. (1959). *Theory of Plates and Shells.* New York: McGraw-Hill.

von Kármán, T., Sechler, E., & Donnell, L. (1932). *The Strength of Thin Plates in Compression.* Transactions of the American Society of Mechanical Engineers (ASME), Vol. 54, p. 53.

7. Annex

A. Energy methods

When using the energy method there are several methods used to solve the problem of the Principal of Minimum Potential Energy which are the Rayleigh-Ritz method and the Galerkin method.

The Rayleigh-Ritz method (Pilkey & Wunderlich, 1994) uses an approximation of the deflection (7.1):

$$\bar{u}_j = \sum_{i=1}^{n_j} q_{ji}\psi_{ji} \tag{7.1}$$

Where q_{ji} are unknown parameters that are to be found and ψ_{ji} are the shape functions. The Rayleigh-Ritz method has the particularity that the solution used only verifies the kinematic boundary conditions of the plate.

By applying the Principal of Minimum Potential Energy the critical load can be calculated. In other words, the total potential energy (V) (7.2) is equal to the sum of the deformation energy (U) and the potential energy of the applied loads (V_e) (it is the inverse of the work done by the loads applied on the structure) and then by minimizing the total potential energy with respect to the parameters (q_{ji}) of the deflection solution, the critical load is given (7.3)

$$V = U + V_e \tag{7.2}$$

$$\frac{\partial U}{\partial q_i} + \frac{\partial V_e}{\partial q_i} = 0 \tag{7.3}$$

This energetic method is an upper bound method because the solution used only satisfies the kinematic boundary conditions so by constraining the structure to deform like the solution assumed, it will increase the stiffness of the structure so that's why the critical load calculated is an upper bound solution of the problem (Reis & Camotim, 2001).

Though the Rayleigh-Ritz method uses an approximated solution the results can be very satisfactory because the approximated solution can have more than one mode of deformation (equation (7.1)).

Other energy method that can be used is the Galerkin method (Pilkey & Wunderlich, 1994). This method also uses an approximation of the solution of the differential equation but in this case instead of only verifying the kinematic conditions, it verifies all boundary conditions: kinematic and equilibrium.

Then, by replacing it in the differential equation, the new solution will give a residual. The goal now is to minimize that residual by multiplying it by the shape functions, now called weights, that constitute the solution used and by integrating it over the domain and then equalizing it to zero.

So depending on the weights chosen, the approximate solution will approach the exact solution.

B. EC3: Case I: $P_{cr,z}=P_{cr,y}=P_{cr,local}$

The column's geometric properties are given by Table 7.1.

Table 7.1: Column's geometric properties and theoretical buckling loads.

L (m)	29.4
h m)	0.950
b (m)	0.850
tw (m)	0.019
tf (m)	0.030
A (m2)	0.0685
i_y (m)	0.4294
I_{yy} (m4)	0.0126
λ_y	68.4669
i_z (m)	0.2118
I_{zz} (m4)	0.0031
λ_z	69.4144
$P_{cr,y}$ (MN)	30.28
$P_{cr,y,ef}$ (MN)	29.66
$P_{cr,z}$ (MN)	29.46
$P_{cr,z,ef}$ (MN)	29.21
$P_{cr,local}$ (MN)	30.83

The classifications of the cross-sections accordingly to the EC3 are presented by Table 7.2:

Table 7.2: Cross-section classification.

Cross-section classifications	
Class	4
Internal compression parts	
ε	0.82
c/t	48.42
Outstand flanges	
c/t	13.85

Table 7.3 presents the EC3 calculations for the buckling resistance without considering the effective width:

Table 7.3: EC3 buckling resistance without considering the effective width.

Buckling Resistance - Global	
$N_{b,Rd}$ (kN)	14454.12
$\sigma_{b,Rd}$ (MPa)	211.07
Buckling curve	c
χ	0.5946
A (m2)	0.0685
α	0.49
ϕ	1.0864
σ_y (MPa)	355
γ_{M1}	1
$N_{cr,z}$ (kN)	29456.63
$N_{cr,y}$ (kN)	30277.58
$L_{cr,z}$ (m)	14.70
$L_{cr,y}$ (m)	29.40
λ_1	76.3986
$\overline{\lambda_z}$	0.9086
$\overline{\lambda_y}$	0.8962

Table 7.4 shows how the EC3 takes into account the fact that the cross-section is class 4.

Table 7.4: The effective width by the EC3

Effective area - EC3 1.5 - 4.4	
Web	
$\overline{\lambda_p}$	1.0478
k_σ	4
ψ	1
ρ	0.7540
t_w (m)	0.0190
b_w (m)	0.9200
b_{eff} (m)	0.6937
A_{eff} (m2)	0.0132
Flange	
$\overline{\lambda_p}$	0.9141
k_σ	0.43
ψ	1

ρ	0.8690
c (m)	0.4155
t_f (m)	0.0300
b_{eff} (m)	0.3611
A_{eff} (m2)	0.0108

Finally the ultimate load given by the Eurocode is shown in Table 7.5.

Table 7.5: Design buckling resistance of a compressed member by the EC3.

Buckling Resistance - Interaction (global and local)	
$N_{b,Rd}$ (MN)	12.96
$\sigma_{b,Rd}$ (MPa)	189.31
$\overline{\lambda_z}$	0.8254
$\overline{\lambda_y}$	0.8141
Buckling curve	c
χ	0.6462
A_{eff} (m2)	0.0565
α	0.49
ϕ	0.9938
σ_y (MPa)	355
γ_{M1}	1
N_{cr} (MN)	29.46
L_{cr} (m)	14.70
λ_1	76.3986
$\bar{\lambda}$	0.8254

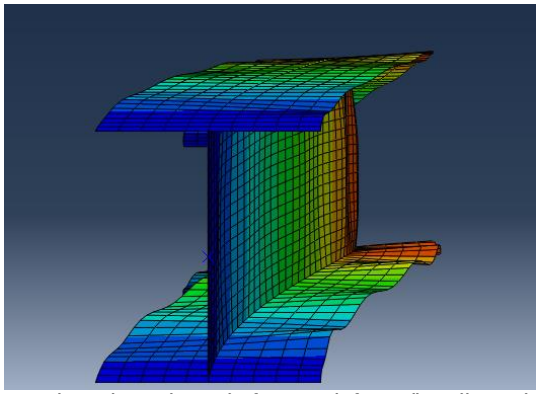

Figure 7.1: Deformed shape when the column is free to deform (locally and globally) for Pcr,global,z= Pcr,global,y= Pcr,local.

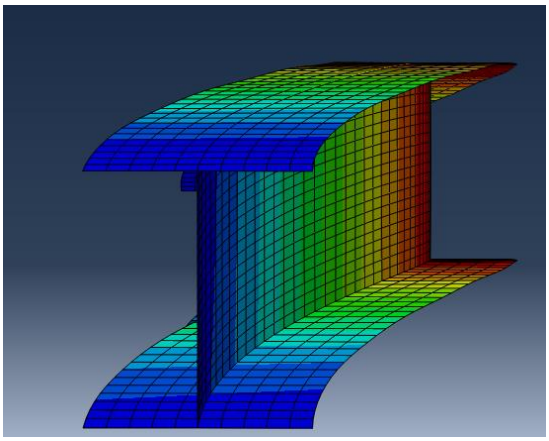

Figure 7.2: Deformed shape when the column is free to deform globally without in-plane deformations for Pcr,global,z= Pcr,global,y= Pcr,local.

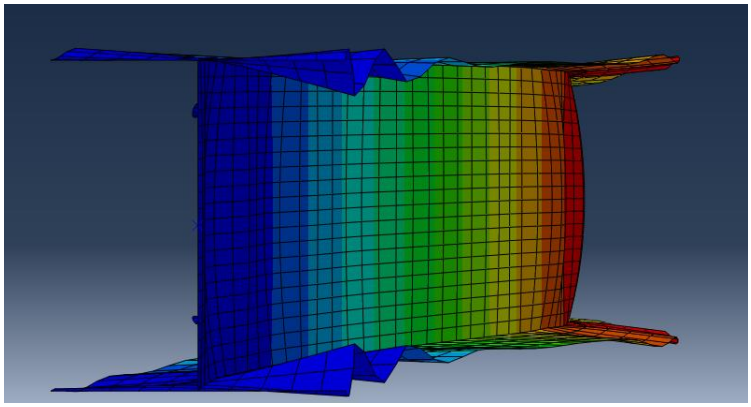

Figure 7.3: Deformed shape when the column can only buckle around the z-axis and in-plane deformations are allowed for Pcr,global,z= Pcr,global,y= Pcr,local.

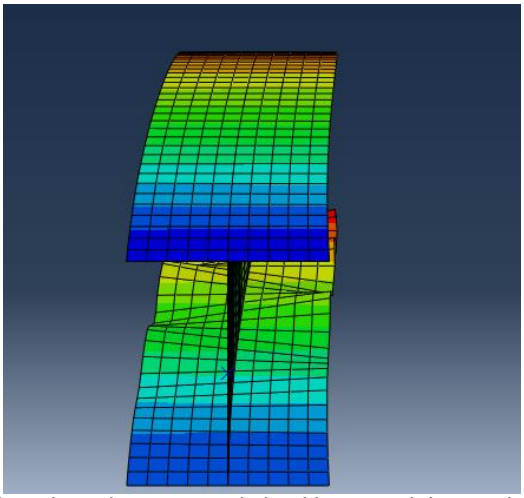

Figure 7.4: Deformed shape when the column can only buckle around the y-axis and in-plane deformations are allowed for Pcr,global,z= Pcr,global,y= Pcr,local.

C. EC3: Case II: $P_{cr,z}=P_{cr,y}<P_{cr,local}$

The column's geometric properties are given by Table 7.6:

Table 7.6: Column's geometric properties and theoretical buckling loads.

L (m)	34
h m)	0.95
b (m)	0.85
tw (m)	0.019
tf (m)	0.03
A (m2)	0.0685
i_y (m)	0.4294
I_{yy} (m4)	0.0126
λ_y	79.1794
i_z (m)	0.2118
I_{zz} (m4)	0.0031
λ_z	80.2752
$P_{cr,y}$ (MN)	22.64
$P_{cr,y,ef}$ (MN)	22.29
$P_{cr,z}$ (MN)	22.03
$P_{cr,z,ef}$ (MN)	21.88
$P_{cr,local}$ (MN)	30.83

The classification of the cross-section accordingly to the EC3 is presented in Table 7.7.

Table 7.7: Cross-section classification.

Cross-section classifications	
Class	4
Internal compression parts	
ε	0.8136
c/t	48.4211
Outstand flanges	
c/t	13.8500

The EC3 calculations without taking into account local buckling (effective width) are given by Table 7.8:

Table 7.8: EC3 calculations without local buckling.

Buckling Resistance - Global	
$N_{b,Rd}$ (kN)	12424.39
$\sigma_{b,Rd}$ (MPa)	181.43
Buckling curve	c
χ	0.5111
A (m2)	0.0685
α	0.49
ϕ	1.2605
σ_y (MPa)	355
γ_{M1}	1
$N_{cr,z}$ (kN)	22025.20
$N_{cr,y}$ (kN)	22639.04
$L_{cr,z}$ (m)	17.00
$L_{cr,y}$ (m)	34.00
λ_1	76.3986
$\overline{\lambda_z}$	1.0507
$\overline{\lambda_y}$	1.0364

Table 7.9 shows how the EC3 takes into account the fact that the cross-section is class 4.

Table 7.9: The effective width by the EC3

Effective area - EC3 1.5 - 4.4	
Web	
$\overline{\lambda_p}$	1.0478
k_σ	4
ψ	1
ρ	0.7540
t_w (m)	0.0190
b_w (m)	0.9200
b_{eff} (m)	0.6937
A_{eff} (m2)	0.0132
Flange	
$\overline{\lambda_p}$	0.9141
k_σ	0.43
ψ	1

ρ	0.8690
c (m)	0.4155
t_f (m)	0.0300
b_{eff} (m)	0.3611
A_{eff} (m2)	0.0108

Finally the ultimate load given by the Eurocode is shown in Table 7.10.

Table 7.10: Design buckling resistance of a compressed member by the EC3.

Buckling Resistance - Interaction (global and local)	
$N_{b,Rd}$ (MN)	11.37
$\sigma_{b,Rd}$ (MPa)	166.03
$\overline{\lambda_z}$	2.1448
$\overline{\lambda_y}$	2.1155
Buckling curve	c
χ	0.5668
A_{eff} (m2)	0.0565
α	0.49
ϕ	1.1404
σ_y (MPa)	355
γ_{M1}	1
N_{cr} (MN)	22.03
L_{cr} (m)	17.00
λ_1	76.3986
$\bar{\lambda}$	0.9545

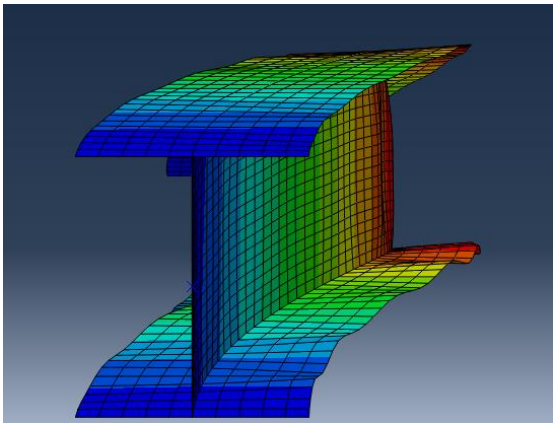

Figure 7.5: Deformed shape when the column is free to deform It's possible to see interaction between local and global modes for Pcr,global,z= Pcr,global,y< Pcr,local.

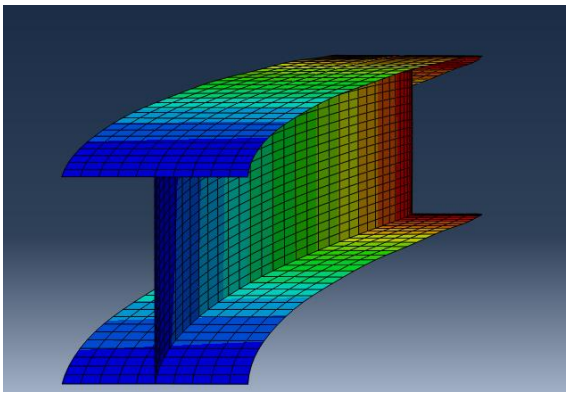

Figure 7.6: Deformed shape when the column is free to deform globally without in-plane for Pcr,global,z= Pcr,global,y< Pcr,local.

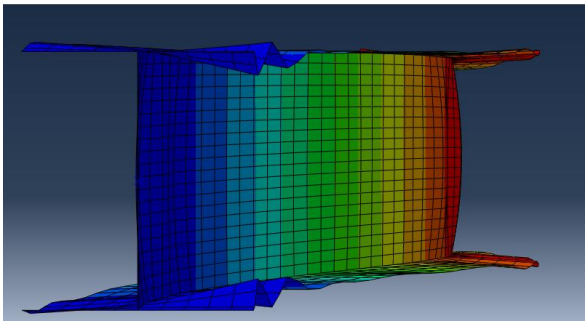

Figure 7.7: Deformed shape when the column can only buckle around the z-axis and in-plane deformations are allowed for for Pcr,global,z= Pcr,global,y< Pcr,local.

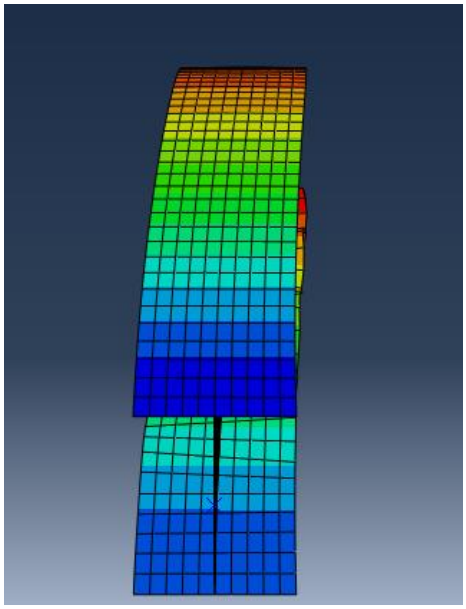

Figure 7.8: Deformed shape when the column can only buckle around the y-axis and in-plane deformations are allowed for for Pcr,global,z= Pcr,global,y< Pcr,local.

D. EC3: Case III: $P_{cr,z}=P_{cr,y}>P_{cr,local}$

The column's geometric properties are given by Table 7.11:

Table 7.11: Column's geometric properties and theoretical buckling loads.

L (m)	22
h m)	0.95
b (m)	0.85
tw (m)	0.019
tf (m)	0.03
A (m2)	0.0685
i_y (m)	0.4294
I_{yy} (m4)	0.0126
λ_y	51.2338
i_z (m)	0.2118
I_{zz} (m4)	0.0031
λ_z	103.8856
$P_{cr,y}$ (MN)	54.07
$P_{cr,y,ef}$ (MN)	52.14
$P_{cr,z}$ (MN)	52.61
$P_{cr,z,ef}$ (MN)	51.81
$P_{cr,local}$ (MN)	30.83

The classification of the cross-section accordingly to the EC3 is given by Table 7.12.

Table 7.12: Cross-section classification.

Cross-section classifications	
Class	4
Internal compression parts	
ε	0.8136
c/t	48.4211
Outstand flanges	
c/t	13.8500

The EC3 calculations without taking into account local buckling are presented by Table 7.13:

Table 7.13: EC3 calculations without local buckling.

Buckling Resistance - Global	
$N_{b,Rd}$ (kN)	17919.10
$\sigma_{b,Rd}$ (MPa)	261.67
Buckling curve	c
χ	0.7371
A (m2)	0.0685
α	0.49
ϕ	0.8487
σ_y (MPa)	355
γ_{M1}	1
$N_{cr,z}$ (kN)	52605.65
$N_{cr,y}$ (kN)	54071.75
$L_{cr,z}$ (m)	11.00
$L_{cr,y}$ (m)	22.00
λ_1	76.3986
$\overline{\lambda_z}$	0.6799
$\overline{\lambda_y}$	0.6706

Table 7.14 shows how the EC3 takes into account the fact that the cross-section is class 4.

Table 7.14: The effective width by the EC3

Effective area - EC3 1.5 - 4.4	
Web	
$\overline{\lambda_p}$	1.0478
k_σ	4
ψ	1
ρ	0.7540
t_w (m)	0.0190
b_w (m)	0.9200
b_{eff} (m)	0.6937
A_{eff} (m2)	0.0132
Flange	
$\overline{\lambda_p}$	0.9141
k_σ	0.43
ψ	1
ρ	0.8690

c (m)	0.4155
t_f (m)	0.0300
b_{eff} (m)	0.3611
A_{eff} (m2)	0.0108

Finally the ultimate load given by the Eurocode is shown in the Table 7.15.

Table 7.15: Design buckling resistance of a compression member by the EC3.

Buckling Resistance - Interaction (global and local)	
$N_{b,Rd}$ (MN)	15.54
$\sigma_{b,Rd}$ (MPa)	227.00
$\overline{\lambda_z}$	2.1448
$\overline{\lambda_y}$	2.1155
Buckling curve	c
χ	0.7749
A_{eff} (m2)	0.0565
α	0.49
ϕ	0.7930
σ_y (MPa)	355
γ_{M1}	1
N_{cr} (MN)	52.61
L_{cr} (m)	11.00
λ_1	76.3986
$\bar{\lambda}$	0.6176

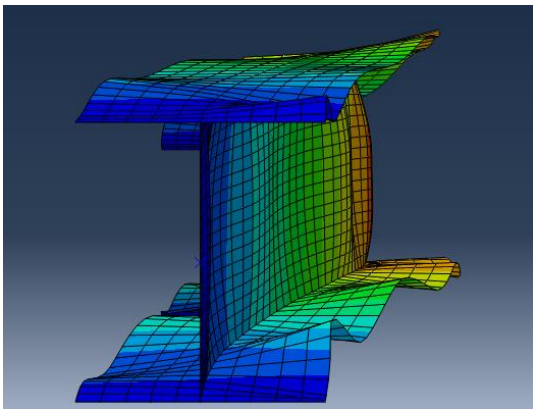

Figure 7.9: Deformed shape when the column is free to deform It's possible to see interaction between local and global modes for Pcr,global,z= Pcr,global,y> Pcr,local.

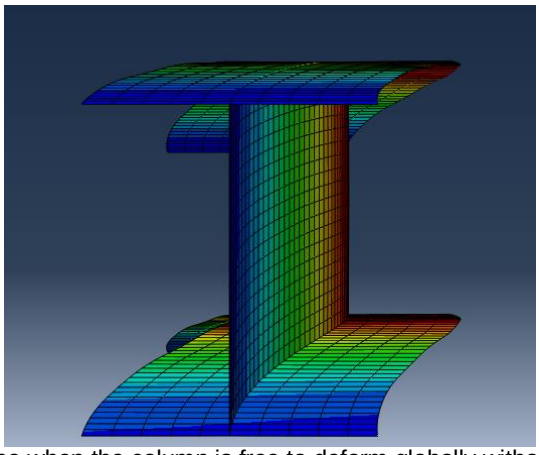

Figure 7.10: Deformed shape when the column is free to deform globally without in-plane deformations for Pcr,global,z= Pcr,global,y> Pcr,local.

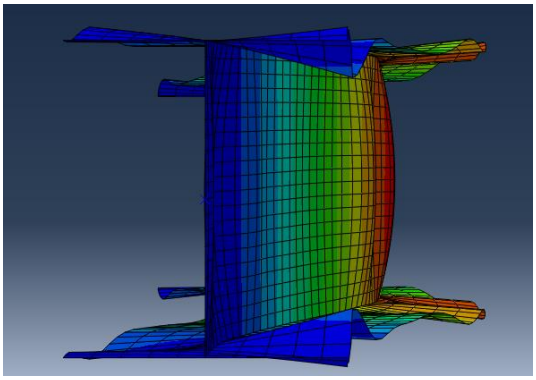

Figure 7.11: Deformed shape when the column can only buckle around the z-axis and in-plane deformations are allowed for for Pcr,global,z= Pcr,global,y> Pcr,local.

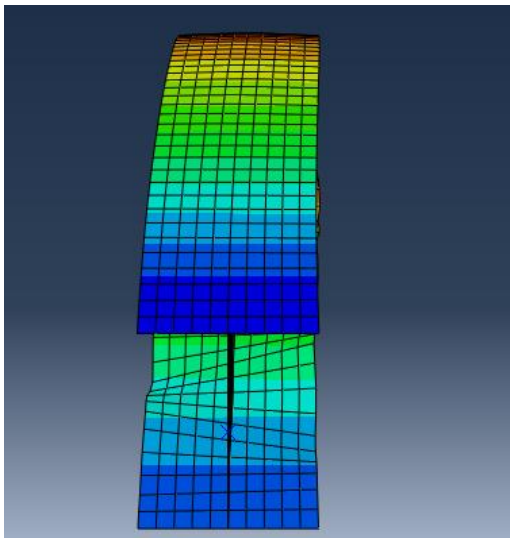

Figure 7.12: Deformed shape when the column can only buckle around the y-axis and in-plane deformations are allowed for for Pcr,global,z= Pcr,global,y> Pcr,local.

E. Interaction between global modes

Considering the same column used in Case I ($P_{cr,global,z}$= $P_{cr,global,y}$= $P_{cr,local}$), this time the column will have its ends fixed in both directions. Therefore the buckling load for the major axis is much higher than the one from the minor axis. The local and global buckling loads are given in Table 7.16.

Table 7.16: Buckling loads from an example where there is no interaction between global modes.

$P_{cr,local}$ (MN)	31.528
$P_{cr,global,z}$ (MN)	29.136
$P_{cr,global,y}$ (MN)	121.110

Then a load – axial shortening path was performed considering the three FE models: interaction between local and global modes; interaction between local and global,z modes; interaction between local and global,y modes. The results are shown in Figure 7.13.

It is possible to see from Figure 7.13 to Figure 7.15 that a column with one buckling load higher than the other, the load path is only affected by the governing global buckling mode and the local buckling mode.

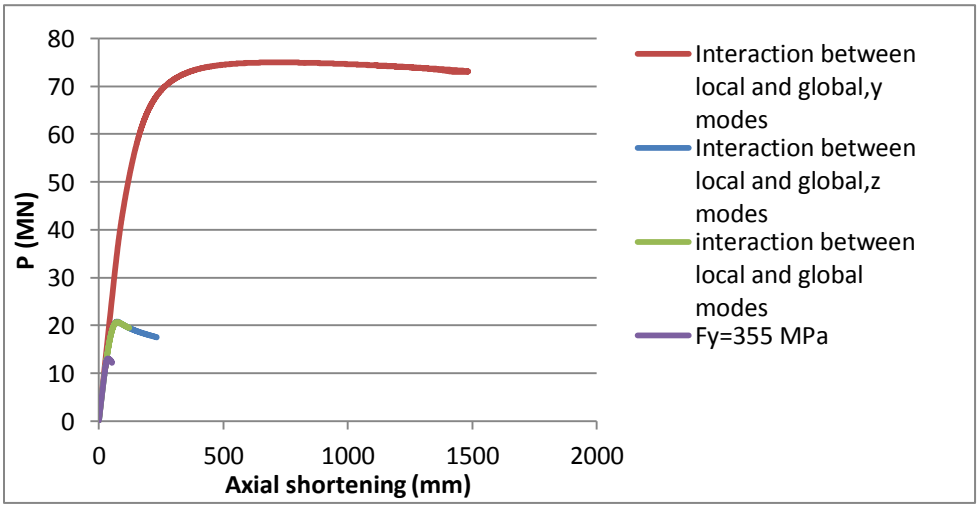

Figure 7.13: Load-axial shortening for Pcr,global,z = Pcr,local< Pcr,global,y .

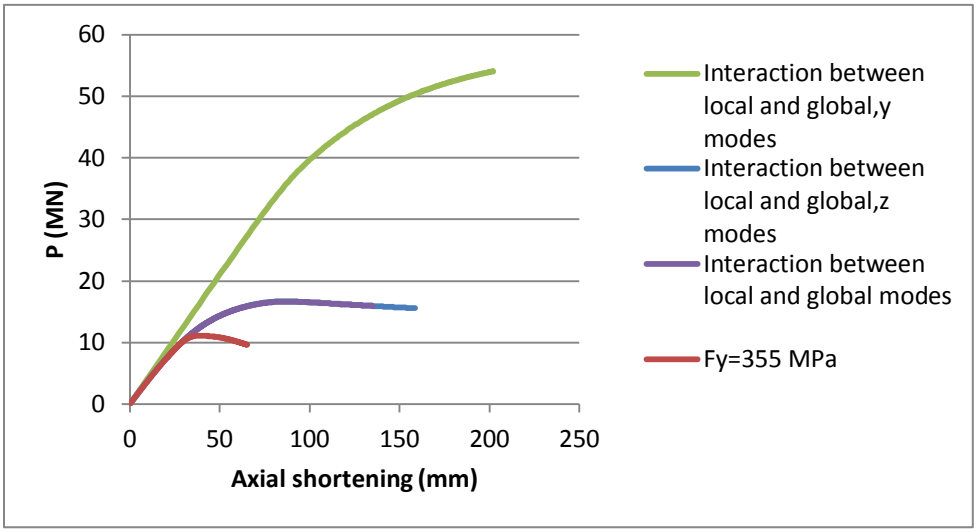

Figure 7.14: Load-axial shortening for Pcr,global,z <Pcr,local< Pcr,global,y

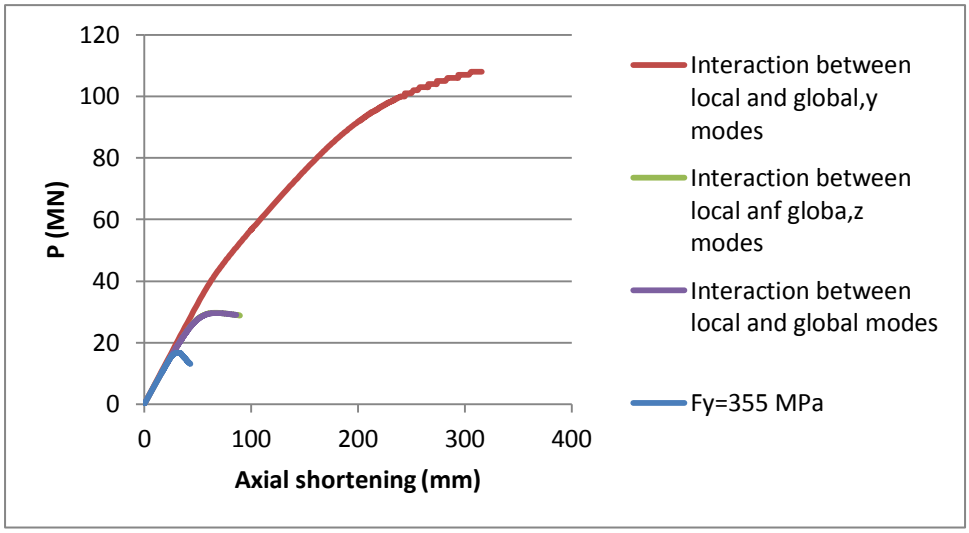

Figure 7.15: Load-axial shortening for Pcr,local < Pcr,global,z < Pcr,global,y.

F. Parametric study the column example

Using the same column cross-section properties from the Case I ($P_{cr,global,z}$= $P_{cr,global,y}$= $P_{cr,local}$), Case II ($P_{cr,global,z}$= $P_{cr,global,y}$< $P_{cr,local}$) and Case III ($P_{cr,global,z}$= $P_{cr,global,y}$> $P_{cr,local}$), a parametric study was developed.

The cross-section is still of class 4 so the same principles of the effective width are applied to calculate the ultimate bearing capacity of the column.

Table 7.17 has, for a range of lengths, the ultimate load capacity obtained by the Eurocode.

Table 7.17: EC3 design buckling resistance.

EC3				
L (m)	$\overline{\lambda_z}$	**ϕ**	**χ**	**$N_{b,Rd}$ (MN)**
10	0.2807	0.5592	0.9590	19.24
11	0.3088	0.5743	0.9447	18.95
12	0.3369	0.5903	0.9302	18.66
13	0.3650	0.6070	0.9157	18.37
14	0.3930	0.6245	0.9010	18.07
15	0.4211	0.6428	0.8861	17.78
16	0.4492	0.6619	0.8710	17.47
17	0.4772	0.6818	0.8556	17.16
18	0.5053	0.7025	0.8400	16.85
19	0.5334	0.7239	0.8241	16.53
20	0.5615	0.7462	0.8080	16.21
21	0.5895	0.7692	0.7916	15.88
22	0.6176	0.7930	0.7749	15.54
23	0.6457	0.8176	0.7580	15.21
24	0.6738	0.8430	0.7409	14.86
25	0.7018	0.8692	0.7236	14.51
26	0.7299	0.8962	0.7061	14.16
27	0.7580	0.9240	0.6885	13.81
28	0.7861	0.9525	0.6709	13.46
29	0.8141	0.9819	0.6533	13.11
30	0.8422	1.0120	0.6357	12.75
31	0.8703	1.0429	0.6182	12.40
32	0.8983	1.0746	0.6008	12.05
33	0.9264	1.1071	0.5837	11.71

34	0.9545	1.1404	0.5668	11.37
35	0.9826	1.1744	0.5501	11.04
36	1.0106	1.2093	0.5338	10.71
37	1.0387	1.2449	0.5178	10.39
38	1.0668	1.2814	0.5022	10.07
39	1.0949	1.3186	0.4870	9.77
40	1.1229	1.3566	0.4722	9.47
41	1.1510	1.3954	0.4578	9.18
42	1.1791	1.4350	0.4439	8.90
43	1.2071	1.4754	0.4304	8.63
44	1.2352	1.5165	0.4173	8.37
45	1.2633	1.5585	0.4047	8.12
46	1.2914	1.6012	0.3925	7.87
47	1.3194	1.6447	0.3807	7.64
48	1.3475	1.6890	0.3694	7.41
49	1.3756	1.7341	0.3584	7.19
50	1.4037	1.7800	0.3479	6.98
51	1.4317	1.8267	0.3377	6.77
52	1.4598	1.8742	0.3279	6.58
53	1.4879	1.9224	0.3185	6.39
54	1.5160	1.9715	0.3094	6.21
55	1.5440	2.0213	0.3007	6.03
56	1.5721	2.0719	0.2923	5.86
57	1.6002	2.1233	0.2842	5.70
58	1.6282	2.1755	0.2764	5.54
59	1.6563	2.2285	0.2689	5.39
60	1.6844	2.2823	0.2616	5.25
70	1.9651	2.8633	0.2022	4.06

Table 7.18 presents the results obtained from FE analyses performed for the parametric study.

Table 7.18: FE parametric study.

L (m)	P_u interaction between modes (MN)	P_u interaction between modes without local imperfections (MN)	P_u interaction between global modes without local imperfections (MN)	P_u without in-plane deformations (MN)	P_u interaction between modes without global,y imperfections (MN)	P_u interaction between global modes without global,y imperfections (MN)	P_u interaction between global modes without global,z imperfections (MN)
10	20.70	21.5	22.2	22.20	21.60	22.30	22.9
14	19.30	20.1	20.6	20.60	20.50	20.80	22.1
18	17.90	18.3	18.7	18.70	18.90	19.00	21
22	16.20	16.4	16.6	16.60	16.90	16.80	19.7
26	14.30	14.4	14.5	14.50	14.80	14.80	18.2
30	12.50	12.5	12.6	12.60	12.90	12.90	16.5
34	10.80	10.9	11	11.00	11.20	11.20	14.7
38	9.44	9.45	9.54	9.55	9.72	9.77	12.7
42	8.26	8.26	8.33	8.34	8.54	8.55	11.2
46	7.25	7.26	7.32	7.32	7.50	7.51	9.8
50	6.41	6.41	6.46	6.46	6.63	6.63	8.58
54	5.69	5.69	5.71	5.73	5.89	5.89	7.55
58	5.08	5.08	5.09	5.11	5.26	5.26	6.67